

A method for quantifying, visualising, and analysing gastropod shell form

Quantitative analysis of organismal form is an important component for almost every branch of biology. Although generally considered an easily-measurable structure, the quantification of gastropod shell form is still a challenge because shells lack homologous structures and have a spiral form that is difficult to capture with linear measurements. In view of this, we adopt the idea of theoretical modelling of shell form, in which the shell form is the product of aperture ontogeny profiles in terms of aperture growth trajectory that is quantified as curvature and torsion, and of aperture form that is represented by size and shape. We develop a workflow for the analysis of shell forms based on the aperture ontogeny profile, starting from the procedure of data preparation (retopologising the shell model), via data acquisition (calculation of aperture growth trajectory, aperture form and ontogeny axis), and data presentation (qualitative comparison between shell forms) and ending with data analysis (quantitative comparison between shell forms). We evaluate our methods on representative shells of the genus *Opisthostoma* and *Plectostoma*, which exhibit great variability in shell form. The outcome suggests that our method is robust, reproducible, and versatile for the analysis of shell form. Finally, we propose several potential applications of our methods in functional morphology, theoretical modelling, taxonomy, and evolutionary biology.

1 Thor-Seng Liew and Menno Schilthuizen

2 1 Institute Biology Leiden, Leiden University, P.O. Box 9516, 2300 RA Leiden, The Netherlands.

3 2 Naturalis Biodiversity Center, P.O. Box 9517, 2300 RA Leiden, The Netherlands.

4 3 Institute for Tropical Biology and Conservation, Universiti Malaysia Sabah, Jalan UMS, 88400,
5 Kota Kinabalu, Sabah, Malaysia.

6 Email: T-S L: thorsengliew@gmail.com

7 MS: Menno.Schilthuizen@naturalis.nl

8 **Funding:** This study is funded under project 819.01.012 of Research Council for Earth and Life
9 Sciences (ALW-NWO). The funders had no role in study design, data collection and analysis,
10 decision to publish, or preparation of the manuscript.

11 **Competing interests:** The authors have declared that no competing interests exist.

12 **Introduction**

13 **Empirical and theoretical approaches in the study of shell form**

14 The external form diversity of organisms is the most obvious evidence for their evolution, and
15 thus is a key element in most branches of biology. The Molluscan shell has been a popular
16 example in morphological evolution studies because it is geometrically simple, yet diverse in
17 form. The shell form is controlled by the shell ontogenetic process, which follows a simple
18 accretionary growth mode where new shell material is accumulatively deposited to the existing
19 aperture. The evolution of shell forms has been studied either by using empirical approaches that
20 focus on the quantification of actual shell forms or by using theoretical approaches that focus on
21 the simulation of shell ontogenetic processes and geometric forms.

22 Notwithstanding the active development in both empirical and theoretical approaches to the study
23 of shell form, there has been very little integration between both schools. For the empirical
24 approach, the quantification methods of shell form have evolved from traditional linear
25 measurement to landmark-based geometric morphometrics and outline analyses (for an overview
26 see Van Bocxlaer & Schultheiß, 2010). At the same time, for the theoretical approach, the
27 simulations of shell form have evolved from simple geometry models that aimed to reproduce the
28 form, to more comprehensive models that simulate shell ontogenetic processes (for an overview
29 see Urdy et al., 2010). Hence, each of the two approaches has been moving forward but away
30 from each other, where synthesis between the two schools of shell morphologists has become
31 more challenging.

32 In empirical morphological studies, shell form, either in terms of heights and widths in traditional
33 morphometrics or in terms of geometry of procrustes distances in geometric morphometrics, is
34 quantified by a set of homologous reference points or landmarks on the shell, which can be easily
35 obtained from the fixed dimensions of the shell. Thus, both methods could abstract the shell form
36 in terms of size and shape of the particular shell dimensions, and the between-sample variation of
37 shell size and shape can be assessed (in most cases only within one study). On the other hand, it
38 is not possible to reconstruct the actual shell form from these quantitative measurements, because
39 the shell's accretionary growth model and spiral geometry cannot be quantified on the basis of
40 arbitrary reference points or fixed dimensions (Stone. 1997). Nevertheless, the traditional and
41 geometric morphometric methods have been accepted widely as standard quantification methods
42 for shell form in many different fields of research.

43 In contrast to empirical morphometrics in which the aim is to quantify the actual shell, theoretical
44 morphologists focus on the simulation of an accretionary growth process which produces a shell
45 form that is similar to actual shells. This field was established with the theoretical shell model of
46 D.M. Raup (Raup, 1961; Raup & Michelson, 1965). Within the first two decades after these
47 publications, only a few different versions of shell models were proposed (e.g. Løvtrup & von
48 Sydow, 1974; Bayer, 1978; McGhee, 1978; Kawaguchi, 1982; Illert, 1983). The subsequent two
49 decades, thanks to the popularity and power of desktop computing, many more theoretical shell
50 models were published (e.g., Savazzi, 1985; Okamoto, 1988; Cortie, 1989; Ackerly, 1989a;
51 Savazzi, 1990; Checa, 1991; Fowler et al., 1992; Illert & Pickover, 1992; Checa & Aguado, 1992;
52 Cortie, 1993; Savazzi, 1993; Rice, 1998; Ubukata, 2001; Galbraith, Prusinkiewicz & Wyvill,
53 2002). Finally, we saw further improvements in the published theoretical models in recent years.
54 These recent models simulate shell forms that more accurately resemble actual shells because of
55 improved programming software, better algorithms, and 3D technology (e.g. Picado, 2009,
56 Stepień, 2009; Meinhardt, 2009; Urdy et al., 2010; Harary & Tal, 2011; Moulton & Goriely,
57 2012; Moulton, Goriely & Chirat, 2012; Faghih Shojaei et al., 2012; Chacon, 2012). Here, we
58 will not further discuss the details of the at least 29 published shell models, but refer to the
59 comprehensive overviews and descriptions of these models in Dera et al. (2009) and Urdy et al.
60 (2010).

61 In brief, the latest theoretical shell models are able to simulate irregularly-coiled shell forms and
62 ornamentations that resemble actual shells, whereas the earlier models could only simulate the
63 regular and general shape of shells. The major refinements that have been made during the almost
64 five decades' development of theoretical shell models are the following modifications of the
65 algorithm: 1) from a fixed reference frame to a moving reference frame system; 2) from
66 modelling based on numerical geometry parameters to growth-parameter-based modelling (e.g.
67 growth rates); 3) from three parameters to more than three parameters, which has made fine-
68 tuning of the shell simulation (e.g. aperture shape) possible. The key element of the theoretical
69 modelling of shells is the generation of shell form by simulating the aperture ontogeny in terms
70 of growth trajectory and form along the shell ontogeny. Hence, this has an advantage over the
71 empirical approach in the numerical representation of the shell geometry form in terms of the 3D
72 quantification and the actual shell ontogenetic processes.

73 Since the empirical and theoretical researchers studying shell form with two totally different
74 quantification methods, our understanding of shell evolution cannot progress solely by using
75 either empirical morphometrics or theoretical models. Ideally, theoretical models need to be
76 evaluated by empirical data of shell morphometrics, and, vice-versa, empirical morphometric
77 methods need to be improved to obtain data that better reflect the actual shell form and
78 morphogenesis which can then be used to improve the theoretical models. In this dilemma lies
79 the central problem of shell form quantification and it urgently needs to be addressed in order to
80 integrate and generalise studies of shell form evolution.

81 **Why empirical morphologists rarely use theoretical shell models**

82 Despite the fact that, since the 1980s, many shell models have been published that are more
83 complex and versatile, the first theoretical shell model of Raup still remains the most popular.
84 There were many attempts by empirical morphologists to use the original or a modified version
85 of Raup's parameters to quantify natural shell forms (e.g. Raup, 1967; Vermeij, 1971; Davoli &
86 Rosso, 1974; Graus, 1974; Kohn & Riggs, 1975; Newkirk & Doyle, 1975; Warburton, 1979;
87 Cameron, 1981; Verduin, 1982; Ekaratne & Crisp, 1983; Saunders & Shapiro, 1986; Tissot, 1988;
88 Foote & Cowie, 1988; Johnston, Tabachnick & Bookstein, 1991; Emberton, 1994; Clarke,
89 Grahame & Mill, 1999; Samadi, David & Jarne, 2000). Surprisingly, all the other shell models,
90 many of which produce more realistic forms, have received very little attention as compared to
91 Raup's model (see e.g. Savazzi, 1992; Okajima & Chiba, 2011; Okajima & Chiba, 2012, for
92 exceptions). This ironic situation might be explained by the elegance of Raup's model that is
93 intuitively and mathematically simple to be used by empirical morphologists (mostly biologists),
94 with limited mathematical and programming experience.

95 As discussed above, most of the theoretical models can simulate a shell that has a form
96 resembling the actual shell in a realistic 3D geometry, based on shell ontogeny processes. In
97 contrast, empirical morphometrics can only quantify and compare certain dimensions of actual
98 shells. Clearly, the theoretical approach is better than the empirical approach in its accuracy of
99 shell form quantification, because accurate morphological quantification is essential for
100 functional, ecological and evolutionary studies of shell form. Below, we identify and discuss a
101 few impediments that currently prevent empirical morphologists from adopting the theoretical
102 approach in shell form quantification.

103 First, the requirement of a computation resource was an impediment in the past. These theoretical
104 models may only be implemented in a computation environment. As mentioned above, the
105 advances of computation hardware in speed and 3D graphic technology have promoted the
106 development of more complex theoretical shell models. For example, the current speed and
107 storage of a desktop computer is at least four orders of magnitude greater than those used by
108 Cortie (1993) only two decades ago. Clearly, the computation hardware is no longer an
109 impediment (e.g. Savazzi, 1995) for the application and development of theoretical shell models.

110 Notwithstanding the hardware development, programming skills are still a prerequisite for the
111 implementation of theoretical models. Many of the early models that were published between the
112 1960s and 1990s, used third-generation programming languages such as Fortran and C++, which
113 essentially lack a graphic user interface. This situation has improved now that the simulation of
114 theoretical shell models can be done in fourth-generation programming languages such as
115 Mathematica (e.g. Meinhardt, 2009; Noshita, 2010; Okajima & Chiba, 2011; Okajima & Chiba,
116 2012) and MATLAB (e.g. Boettiger, Ermentrout & Oster, 2009; Urdy et al. 2010, Faghieh Shojaei
117 et al., 2012). Most of these shell models were described with intensive mathematical notation, at
118 least from a biologist's point of view, in the publication; and some of these were published
119 together with the information on algorithm implementation. However, the actual programming
120 codes are rarely published together with the paper though they may be available from the authors
121 upon request (but see Meinhardt, 2009; Noshita, 2010; Okajima & Chiba, 2011). Only one
122 theoretical modelling software package based on Raup's model has a graphic user interface that is
123 comparable to contemporary geometric morphometric software (Noshita, 2010). Thus, the rest of
124 the modern theoretical models are far less approachable than the morphometric software for
125 empirical morphologists. This is because those advanced theoretical models have not been
126 delivered in a form that allowed empirical morphologists to have "hands-on experience" with
127 them, without extensive mathematical literacy (Savazzi, 1995; McGhee, 2007).

128 Second, theoretical shell models simulate the shell form based on the input of a set of parameters,
129 which could be non-biological or/and biologically meaningful. Non-biological meaningful
130 parameters are counter-intuitive for empirical morphologists because these parameters are not
131 extrinsic shell traits. Nevertheless, many of these non-biological parameters are required for the
132 model to fit the shell form schematically (Hutchinson, 1999). When the biological parameters do

133 represent shell traits, they are often difficult to obtain accurately and directly from the actual shell
134 because of the three-dimensional spiral geometry (Cain, 1977; Ackerly, 1989a; Ackerly, 1989b;
135 Okamoto, 1988; Schindel, 1990; Checa & Aguado, 1992, Hutchinson, 1999; McGhee, 1999).
136 Since the development of theoretical shell models, almost all simulated shell models have been
137 made by an ad hoc approach, where the parameters are chosen for the model and then the
138 simulated shells are compared with the actual shells. In almost all cases, the correct parameters
139 are chosen after a series of trial-and-error, and the parameters are selected when the form of the
140 simulated shell matches the actual shell. Okamoto (1988) suggested that this ad hoc approach
141 based on pattern matching was easier than obtaining the parameters empirically from the shell.

142 Third, although the overall forms of the simulated shells resemble the actual shells, the simulated
143 shell is not exactly the same as the actual shell (Kohn & Riggs, 1975; Goodfriend, 1983). For
144 many models, its original parameters are not sufficient to simulate the shell form exactly
145 (Schindel, 1990; Fowler, Meinhardt & Prusinkiewicz, 1992). These simulated general shell forms
146 are adequate for theoretical morphologist interests in their exploration of general shell forms.
147 However, the subtle features on a real shell or the subtle differences among different shell forms
148 of real species that cannot be simulated by theoretical models may have significant functional
149 implications that are important for empirical morphologists.

150 In brief, it is clear that the implementation of current theoretical shell models is less accessible to
151 empirical shell morphologists. Yet, empirical morphologists are using traditional and geometric
152 morphometrics as a routine method for shell quantification.

153 **Why empirical morphologists use traditional and geometric morphometrics**

154 In addition to the impediments arising from the theoretical shell model itself that are limiting its
155 popularity among empirical morphologists, the theoretical approach faces competition from
156 geometric morphometric methodology. The popularisation of desktop computing that led to the
157 flourishing of theoretical shell models in the late 1980s, also promoted the development of
158 morphometric methods, such as Elliptical Fourier Analysis (EFA) and geometric morphometrics
159 (GM). Rohlf and Archie (1984) set a benchmark for the quantification of an organism's form by
160 EFA, which was improved from Kaesler and Waters (1972) and Kuhl and Giardina (1982). Rohlf
161 and Slice (1990) and Bookstein (1991) developed a complete standard protocol for GM. Soon

162 after these pioneer papers, various software with Graphic User Interface (GUI) were developed
163 for the application of EFA and GM (Cardini & Loy, 2013, see <http://life.bio.sunysb.edu/morph/>).
164 In contrast to the application of theoretical shell models, an understanding of mathematics and
165 programming languages is not a prerequisite for the user of these morphometric tools. Thus, EFA
166 and GM have been well received by biologists, and have been adopted in the morphometric study
167 of shell form.

168 These geometric morphometric software packages have standard and interactive workflows that
169 help empirical morphologists in every step of: obtaining morphometric data (e.g. placing
170 landmark coordinates), analysing data (e.g. procrustes superimposition), statistical analysis (e.g.
171 ANOVA, PCA), and visualising shape and shape changes (e.g. thin-plate spline, PCA plots). This
172 has made geometric morphometrics approachable and attractive to empirical morphologists, who
173 want to examine the similarities and differences among shell forms.

174 Geometric morphometrics is actually a statistic of shape that is calculated from Cartesian
175 coordinate data from a sample of objects (Cardini & Loy, 2013). However, it is not an exact
176 quantification of form and is not particularly suitable for comparison and quantification of shell
177 form, for the following two reasons.

178 First, GM analysis is based on homologous landmarks on the form, but shell has only arbitrary
179 landmarks because it has a low degree of morphological complexity (Van Bocxlaer & Schultheiß
180 2010). There are no evolutionary homologies that can be defined as landmarks on a shell, since
181 the helical coiled tube offers no points that can be fixed across different individuals. In most
182 cases, 2D landmarks are chosen at the shell apex, suture, and aperture or whorl outline that can be
183 identified from a 2D image that is taken in standard apertural view of a shell. These landmarks
184 are chosen to be analysed by GM but these points have little biological meaning. Furthermore, as
185 opposed to the form of many other organisms, 3D landmarks are even more difficult to be
186 obtained from a shell (3D model) as compared to 2D landmarks because many of these
187 landmarks, such as suture points, that are obtained from a 2D image are just artefacts of the fixed
188 2D view of the shell.

189 Second, the results of separate, independent studies of shell forms cannot be integrated, even
190 though these studies use the same GM method. Statistical analysis of the Cartesian coordinate

191 data that abstractly represent the shell form is adequate in quantifying the variation of a shell
192 within a context of other shells that are included in a single study or within similar taxa where
193 similar landmarks are obtained. However, the raw coordinate data and analysed shape variation
194 from a study are incomparable and incompatible with the data from other studies (Klingenberg,
195 2013). For example, the raw data (coordinates) from two studies cannot be combined if they use
196 different landmarks and the shape variables (e.g. PCA scores) from a study cannot be compared
197 and analysed together with other studies.

198 Despite the fact that geometric morphometrics has been widely used by empirical morphologists,
199 it is not an ideal tool in the quantification of shell form for the reasons given above. The
200 increasing availability of the software and application in the literature might cause morphologists
201 to stray away from their initial aims of studying shell form. Hence, it is important to return to the
202 core of the question: what do biologists want to learn from the study of shell form? Clearly, in
203 addition to quantitatively compare shell forms, biologists want to know more about the general
204 characteristics and physical properties of the shell form that are key elements in gaining insight
205 into functional and ecological aspects of the shell (Evans, 2013). However, functional and
206 ecological aspects of shell form can only be determined if the shell form can be exactly
207 quantified.

208 **Using 3D technology to quantify shell form based on aperture ontogeny profiles**

209 In this paper, we propose an interactive approach to the quantification and analysis of shell forms
210 based on state of the art 3D technology and by integrating the theoretical principles of shell
211 modelling and the empirical principles of morphometric data handling. There are no theoretical
212 models that can simulate all existing shell forms. However, the theoretical background of the
213 theoretical models is biologically sound – simulating the shell form by simulating the shell
214 ontogenetic process. On the basis of this shell-ontogenesis principle, we used state-of-the-art X-
215 ray microtomography (micro-CT scan) and 3D modelling software to obtain a series of shell
216 aperture changes from the shell in an interactive workflow that is similar to empirical
217 morphometric analysis.

218 First, a series of shell aperture outlines were digitised directly from the reconstructed 3D shell
219 model obtained from micro-CT scanning by using open-source 3D-modelling software – Blender

220 ver. 2.63 (www.blender.org). Then, the growth trajectory and form of the shell aperture outline
221 were quantified and extracted with our custom scripts that run in Blender through its embedded
222 open-source Python interpreter (<http://www.python.org/>). The changes of aperture size and shape,
223 and aperture growth trajectory in terms of curvature and torsion along the shell ontogeny axis
224 length were obtained (hereafter “aperture ontogeny profiles”). The final aperture ontogeny
225 profiles are in a form of multivariate time series data, which consist of a number of instances (i.e.
226 number of quantified apertures that depends on the length of the whorled shell tube) and
227 attributes that represent the growth trajectories, aperture form, and size.

228 These aperture ontogeny profiles can be plotted when each shell is examined individually. On the
229 other hand, the aperture ontogeny profiles can be visually compared between different shells by
230 plotting the data as radar chart (i.e. spider and star plots). In addition, the differences between
231 shells can be assessed quantitatively by calculating the dissimilarity of aperture ontogeny profiles
232 among shells. Furthermore, the dissimilarity matrix can be used to plot the dendrogram and
233 NMDS plots, which resemble a shell morphospace. All our procedures were implemented by
234 using open source and free software.

235 Finally, we discuss some possible applications and implications of these shell form quantification
236 methods in theoretical morphology, functional morphology, taxonomy and shell shape
237 evolutionary studies.

238 **Materials and Methods**

239 **Ethics Statement**

240 Specimens were collected in Malaysia with permissions from the Economic Planning Unit,
241 Malaysia (UPE: 40/200/19/2524).

242 **Scanning instrumentation**

243 A micro-CT scanner (SkyScan, model 1172, Aartselaar, Belgium) and its accompanying software,
244 NRecon ver. 1.6.6.0 (Skyscan©) and CT Analyser ver. 1.12.0.0 (Skyscan©), were used to
245 generate digital shell 3D models from the actual shell specimens.

246 **Computation software and hardware**

247 Various commercial 3D modelling and statistical software exist for visualising, manipulating, and
248 understanding morphology, such as Amira® (Visage Imaging Inc., San Diego, CA) and Autodesk
249 Maya (San Rafael, CA) (reviewed by Abel, Laurini & Richter, 2012). However, in this study, we
250 used only two open-source 3D data modelling and processing software packages, namely Blender
251 ver. 2.63 (www.blender.org) and Meshlab ver. 1.3.2 (Cignoni, Corsini & Ranzuglia, 2008,
252 <http://meshlab.sourceforge.net/>). Both have been used in biology to visualise and model
253 morphology (for Meshlab: Im et al., 2012; Chaplin, Yu & Ros, 2013; Atwood & Sumrall, 2012;
254 for Blender: Pyka et al., 2010: 22); Haug, Maas & Waloszek, 2009; Cassola et al., 2010; Haug et
255 al., 2010; Andrei et al., 2012; Haug et al., 2012; Lv et al., 2013; Mayer et al., 2012). However,
256 these programs have not been used to their full extent in morphological quantification and
257 analysis of 3D data for organisms. For quantification of morphology, we used the open-source
258 Python interpreter ver. 3.2 that is embedded in Blender 2.63. In addition, we also used an
259 extension to the Python programming language – NumPy (Oliphant, 2007) which consists of
260 high-level mathematical functions.

261 All the morphological data were explored and analysed with the statistical open source
262 programming language R version 3.0.1 (R Core Team, 2013) in the environment of RStudio
263 (RStudio, 2012). We installed three additional packages in R, namely, "lattice": Lattice Graphics
264 (Sarkar, 2008), "pdc": Permutation Distribution Clustering (Brandmaier, 2012a; Brandmaier,
265 2012b), and "fmsb" (Nakazawa, 2010).

266 All the computation analyses were carried out with a regular laptop computer with the following
267 specifications: Intel®Core™i7-3612QM @ 2.1GHz, 8 GB memory (RAM), NVIDIA® GeForce
268 GT 630M with 2GB memory.

269 **Procedures**

270 **1. Obtaining digital 3D models from actual shells**

271 The scan conditions were as follows: voltage – 80kV or 100kV; pixel – 1336 rows × 2000
272 columns; camera binning – 2 × 2; image pixel size – 3–6 μm; rotation step – 0.4° or 0.5°; and
273 rotation – 360°. Next, the volume reconstruction on the acquired images was done in NRecon.
274 The images were aligned to the reference scan and reconstruction was done on the following
275 settings: beam hardening correction – 100%; reconstruction angular range – 360 degree;
276 minimum and maximum for CS to image conversion (dynamic range) – ca. 0.12 and ca. 20.0; and

277 result file type – BMP. Finally, 3D models were created from the reconstruction images in CT
278 Analyser with the following setting: binary image index – 1 to 255 or 70 to 255; and were saved
279 as digital polygon mesh object (*.PLY format).

280 **2. Pre-processing digital shell models**

281 The 3D models were then simplified by quadric edge collapse decimation implemented in
282 MeshLab (Cignoni, Corsini & Ranzuglia, 2008) to reduce computation requirements. The raw
283 polygon mesh shells in PLY format have millions of faces and a file size between 20 to 80
284 Mbytes. Thus, we reduced the number of faces for all model to 200,000 – 300,000 faces, which
285 range between 3 and 6 Mbytes in file size. In addition, for the sake of convenience during the
286 retopology processes, all 3D models were repositioned so that the shell protoconch columella was
287 parallel with the z-axis. This was done by using manipulator tools in MeshLab.

288 **3. Creating reference: Tracing aperture outlines and ontogeny axis from shell models** (Supplementary 289 Information File 1)

290 The digital shell 3D model in PLY format consists of 3D Cartesian coordinate vertices in which
291 each of the three vertices constitutes a triangular face, and all faces are connected through a
292 complex network. In order words, these vertices and faces are not biologically meaningful
293 structures, and it is not possible to extract aperture outlines data directly from a raw PLY digital
294 shell model. Monnet et al. (2009), for example, attempted to extract aperture outline
295 automatically from a digital 3D model by making a plane cross-sectioning of the shell model, but
296 its outlines do not reflect the form of the actual aperture outlines. Hence, we retopologised the
297 raw 3D mesh models according to the aperture ontogeny for later data extraction.

298 We used Blender, which is more flexible than the commercial software used by Monnet et al.
299 (2009). For the sake of convenience, we describe the following workflow, including the tools or
300 the function (e.g. “Import PLY”) which can be called after hitting the SPACE bar while in the
301 Blender environment. However, this workflow may be modified by the user.

302 To begin, we imported a PLY shell model into the Blender environment (“Import PLY”). Then,
303 we resized the model $1000 \times$ (“Resize”) so that the scale of 1 Blender unit was equal to 1 mm.
304 After that, we examined the traces of aperture outlines (i.e. growth lines, ribs, spines) (Figure 1A)
305 and ontogeny axis (i.e. spiral striation, ridges, colour lines) (Figure 1B) of the actual shells.

306 However, it is not possible to trace apertures from the shell protoconch because the protoconch is
307 an embryonic shell that may not grow accretionarily and usually has no growth lines. In many
308 cases, the aperture of the overlapping whorls cannot be traced from the outer shell wall. One of
309 the ways to deal with this situation is to trace the aperture at the inner shell wall and the obscured
310 aperture outline can then be inferred by studying conspecific juvenile specimens (see video
311 tutorial 05:00–08:00 of Supplementary Information File 1). It does not really matter whether the
312 aperture outline was traced from outside or inside. After it was traced from the inside, the
313 subsequent retopologising stage would need take into consideration the shell thickness of the
314 overlapping whorl.

315 After these aperture traits were identified, we selected the 3D model (by clicking “right mouse
316 button”), and traced all these traits on the surface of the raw 3D mesh model in Blender by using
317 the “Grease Pen Draw” tool. After that, the grease pen traced aperture traits were converted to
318 Bezier curves with “Convert Grease Pencil” (Figure 1C). We would like to emphasise that this is
319 the most critical step that determines the efficiency of this shell quantification method. Thus, the
320 key lies in the good understanding of the way the aperture is structured, which is essential to trace
321 the aperture outlines accurately. However, the orientation of the shell when the aperture is
322 digitalised would not influence the aperture ontogeny data.

323 4. Retopologising aperture outlines from the reference and generating retopologised shell models

324 (Supplementary Information File 1 and File 4)

325 For each shell, we created a set of new Non Uniform Rational B-Splines (NURBS) surface
326 circles (“Add Surface Circle”) and modified these (“Toggle Editmode”) according to the aperture
327 outlines. We created a 16 points NURBS surface circle and aligned the circle to the aperture
328 outline by translation (“Translate”), rotation (“Rotate”), and resizing (“Resize”) (Figure 1D).
329 After the NURBS surface circle was generally aligned, each of the 16 points of the NURBS
330 surface circle were selected and adjusted by translation (“G”) one by one, so that the outline of
331 the NURBS surface circle was exactly the same as the aperture outline. At the same time, the
332 second point of the NURBS surface circle was aligned to the ontogeny axis (Figures 1B and 1C).

333 After the first aperture outline was retopologised as a NURBS surface circle, the NURBS surface
334 circle was duplicated (“Duplicate Objects”) and aligned to the next aperture outline as the
335 previous one. This step was repeated until all the aperture outlines were retopologised into

336 NURBS surface circles (Figures 1D and 1E). Then the shell surface was created in the form of a
337 NURBS surface based on the digitised aperture NURBS surface circle (“(De)select All” and
338 “Make Segment” in “Toggle Editmode”) (Figures 1F and 1G). Lastly, we made the surface meet
339 the end points in U direction and increased the surface subdivision per segment (resolution $U = 8$)
340 through the properties menu of the object (Properties (Editor types)>Object Data>Active Spline).

341 After that, we converted the NURBS surface 3D model into a 3D Mesh model that consists of
342 vertices, edges, and faces (“Convert to” - “Mesh from Curve/Meta/Surf/Text”). The final
343 retopologised 3D shell Mesh consists of X number of apertures outlines and each aperture outline
344 has Y number of vertices and then a total of $X*Y$ vertices. Each of the vertices is connected to
345 four other nearest vertices with edges to form a wireframe shell and face (Figure 1H).

346 It is important to note that the NURBS surface circle is defined by a mathematic formula which
347 does not imply any biology perspective of the shell. We choose NURBS surface circle because
348 the 3D aperture outline form can be digitalised by a small number of control points and shell
349 surface can be recreated by NURBS surface based on the digitised aperture NURBS surface
350 circle. The final 3D polygon mesh model is more simplified than the raw PLY 3D model and each
351 of its vertex data resemble the actual accretionary process of the shell (Figures 1A and 1H).

352 **5. Quantifying aperture growth trajectory**

353 The aperture ontogeny profiles were quantified as described in Liew et al. (2014a) with slight
354 modifications where both aperture growth trajectory and aperture form were quantified directly
355 from the retopologised 3D shell model. This aperture growth trajectory was quantified as a spatial
356 curve, which is the ontogeny axis as represented by a series of first points of the aperture outlines.
357 We estimated two differential geometry parameters, namely, curvature (κ) torsion (τ), and
358 ontogeny axis length for all apertures (Okamoto, 1988; Harary & Tal, 2011). The local curvature
359 and torsion, and accumulative ontogeny axis length were estimated from the aperture points
360 along the growth trajectory by using weighted least-squares fitting and local arc length
361 approximation (Lewiner et al., 2005). All the calculations were done with a custom-written
362 Python script which can be implemented in Python interpreter in the Blender ver. 2.63
363 environment. The whole workflow was: (1) selecting the retopologised 3D shell Mesh (by
364 clicking “right mouse button”), (2) input parameters for number of sample points “ $q = \#\#$ ” in the
365 python script, and (3) paste the script into the Python interpreter (Supplementary Information File

366 2). The final outputs with torsion, curvature and ontogeny axis reference for each aperture were
367 saved as CSV files.

368 We found a convergence issue in curvature and torsion estimators. The accuracy of the curvature
369 and torsion estimates depends on the number and density of the vertices in the ontogeny axis (i.e.
370 number of aperture outlines), and the number of sample points. Nevertheless, different numbers
371 of sample points can be adjusted until good (i.e. converged) curvature and torsion estimates are
372 obtained. We used 10% of the total points as number of sample points of the ontogeny axis,
373 which gave reasonably good estimates for curvature and torsion.

374 Notwithstanding the algorithm issue, the curvature and torsion estimators are informative in
375 describing the shell spiral geometry growth trajectory. Curvature is always larger or equal to zero
376 ($\kappa \geq 0$). When $\kappa = 0$, the spatial curve is a straight line; the larger the curvature, the smaller the
377 radius of curvature ($1/\kappa$), and thus the more tightly coiled the spatial curve. On the other hand,
378 the torsion estimator can be zero or take either negative or positive values ($-\infty \leq \tau \leq \infty$). When τ
379 $= 0$, the spatial curve lies completely in one plane (e.g. a flat planispiral shell), negative torsion
380 values correspond to left-handed coiling and to right-handed coiling for positive torsion values;
381 the larger the torsion, the smaller the radius of torsion ($1/\tau$), and thus the taller the spiral.

382 6. Quantifying aperture form

383 We quantified the aperture outline sizes as perimeter and form as normalised Elliptic Fourier
384 coefficients (normalised EFA) by using a custom-written Python script which can be
385 implemented Python interpreter embedded in the Blender environment. The workflow was (1)
386 selecting the retopologised 3D shell mesh (by clicking “right mouse button”), (2) input
387 parameters for “number_of_points_for_each_aperture = ##” in the python script, and (3) paste
388 the script into the Python interpreter of Blender (Supplementary Information File 2). The final
389 outputs were saved as CSV files.

390 Aperture outline perimeter was estimated from the sum of lengths (mm) for all the edges that are
391 connecting the vertices (hereafter “aperture size”). For aperture form analysis, we used 3D
392 normalised EFA algorithms (Godefroy et al., 2012) and implemented these in the custom python
393 script. Although many algorithms exist for describing and quantifying the form of a closed

394 outline (Claude, 2008), we used EFA because it is robust to unequally spaced points, can be
395 normalised for size and orientation, and can capture complex outline form with a small number of
396 harmonics (Rohlf & Archie, 1984; Godefroy et al., 2012). In this study, we used five harmonics,
397 each with six coefficients which were sufficient to capture the diverse aperture shapes of our
398 shells. For quantification of apertures shape that are invariant to size and rotation, we normalised
399 EFA of aperture outlines for orientation and size. If needed for comparison with other studies, the
400 normalised EFA can be repeated for the same dataset with higher or lower numbers of harmonics.

401 After normalisation, we ran principal components analysis (PCA) to summarise the 30
402 normalised Fourier coefficients as principal components scores (hereafter “aperture shape
403 scores”). After that, we selected the major principal components (explaining > 90 % of the
404 variance) for further analysis. The aperture shape scores of each selected principal component
405 were plotted and analysed against the ontogeny axis.

406 **7. Visualising aperture form and trajectory changes along the shell ontogeny**

407 For exploration of data, we used two graphical techniques for representing aperture ontogeny
408 profile changes along the shell ontogeny. For each shell, we made a vertical four-panels scatter
409 plot in which each of the four variables (namely, curvature, torsion, aperture size, and the first
410 principal component aperture shape score) were plotted against the ontogeny axis. When
411 necessary, the second and third principal component aperture shape scores were also included. In
412 addition, the axis of each variable was rescaled so that it was the same for the same variable of all
413 shells. After standardisation of the axis, the aperture ontogeny profiles of several shells could be
414 quantitatively compared side by side.

415 However, comparison of between plots would become less effective with a larger number of
416 shells. Alternatively, therefore, all aperture ontogeny profile variables of each shell can also be
417 represented in a radar chart, instead of scatter plots. This chart is effective in showing the variable
418 outliers within a chart and the overall similarity between charts. Before plotting the data in a
419 radar chart, the datasets of all shells need to be restructured because the dataset of different shells
420 could differ in the number of data points (i.e. quantified aperture), which depends on the
421 ontogeny axis length of each shell.

422 We did this by dividing the ontogeny axis of each shell into 20 equal length intervals, and then by
423 sampling the variable values at the end of every interval. In the restructured dataset, the trend of
424 the aperture ontogeny profile of each variable is retained and all radar charts have the same
425 number of data points. Thus, the changes of aperture variables between each subsequent 1/20 of
426 the ontogeny axis can be examined within a shell and be compared among different shells in a
427 synchronistic manner. We suggest to use 20 points to summarise hundreds variable points of the
428 aperture ontogeny profile variables along ontogeny axis because the radar would be
429 overwhelming with too many points and hard to interpret. Similar to the scatter plot, we
430 standardised the axis scales of each variable of all radar charts.

431 In addition, we added a new variable which represents the ontogeny axis interval length in order
432 to compensate for the loss of shell size information during the standardisation of ontogeny axis
433 length. Finally, we plotted the variables, namely, curvature, torsion, aperture size, and ontogeny
434 axis length, and aperture shape scores in a radar chart for each shell by using the “fmsb” library
435 (Nakazawa, 2010) with R version 3.0.1 (R Core Team, 2013) (Supplementary Information File
436 5).

437 **8. Quantitative comparison between shell forms**

438 In addition to the qualitative comparison between shells forms as described above, the
439 dissimilarity between different shells can be analysed quantitatively. We used Permutation
440 Distribution Clustering (PDC) which finds similarities in a time series dataset (Brandmaier,
441 2012a; Brandmaier, 2012b). PDC can be used for the analysis of the changes in a variable along
442 shell ontogeny between different shells (i.e. two-dimensional dataset: number of shells \times number
443 of apertures) and multiple variable changes between shells (i.e. three-dimensional dataset:
444 number of shells \times number of variables \times number of apertures). We applied the most recent
445 analysis developed by Brandmaier (2012a & b) because it has an R package that can be applied
446 and can calculate the trend similarity. That said, the same data can always be analysed by other
447 “better” algorithms in the future.

448 Although PDC is robust to the length differences between datasets, our preliminary analysis
449 showed that the PDC output would be biased when there was a great (around two-fold) length
450 difference in the total ontogeny axis length. Hence, we standardised the data as in procedure 7,
451 but dividing the ontogeny axis of each shell into 50, instead of 20, equal length intervals. This

452 standardisation procedure allows comparison of trends in variable changes along the shell
453 ontogeny without the influences of size. In other words, the dissimilarity is zero between two
454 shells that have exactly the same shape, but differ only in size. In addition to the shape
455 comparison, we obtained the shell size in terms of volume by using “Volume” function in
456 Blender after the 3D shell model was closed at both ends by creating faces “Make edge/Face”) on
457 selected apertures at both end (“Loop Select”) in EDIT mode.

458 The aperture ontogeny profiles of all shells were combined into a three-dimensional data matrix
459 consisting of n shells \times four variables \times 50 aperture data points. We ran four PDCs, each for the
460 five data matrices with: 1) all four variables, 2) torsion, 3) curvature, 4) aperture size, and 5)
461 aperture shape scores. The parameter settings for the PDC analysis were as follows: embedding
462 dimension = 5; time-delay of the embedding = 1; divergence measure between discrete
463 distributions = symmetric alpha divergence; and hierarchical clustering linkage method = single.
464 The dissimilarity distances between shells were used to produce the dendrogram. PDC analysis
465 was performed with the “pdc” library (Brandmaier, 2012b) in R version 3.0.1 (R Core Team,
466 2013) (Supplementary Information File 5).

467 In addition to the dendrogram representation of the output from PDC, we plotted the dissimilarity
468 as a non-metric multidimensional scaling (NMDS) plot which resembles a morphospace. NMDS
469 was performed by using “MASS” library (Venables & Ripley, 2002) in R version 3.0.1 (R Core
470 Team, 2013) (Supplementary Information File 5).

471 **Worked example: Comparative analysis of *Opisthostoma* and *Plectostoma* species shell form** 472 **and simulated shell form**

473 We evaluated the above-described shell form quantification method by using the shells of
474 *Opisthostoma* and *Plectostoma*, which exhibit a great variability in shell form. Some of the
475 species follow a regular coiling regime whereas others deviate from regular coiling in various
476 degrees. It remains a challenging task to quantify and compare these shell forms among species,
477 either by using traditional or geometric morphometrics, because a standard aperture view for the
478 irregular and open coiled shells cannot be determined.

479 We selected four species, namely, *Plectostoma laidlawi* Skyes 1902 (Figure 2A), *Plectostoma*
480 *crassipupa* van Benthem Jutting, 1952 (Figure 2B), *Plectostoma christae* Maassen 2001 (Figure

481 2C), and *Opisthostoma vermiculum* Clements and Vermeulen, 2008 (in Clements et al., 2008)
482 (Figure 2D), for which the shell forms are, respectively: regularly coiled, slight distortion of the
483 last whorl, strong distortion of the last whorl, and complete distortion of most of the whorls.
484 Despite the narrow taxonomic range of the selected species, the range of shell forms of these four
485 species do cover a very large diversity of shell form. We retopologised these four shells by
486 following the procedures 1 to 4 (Supplementary Information Files 6).

487 In addition to the four retopologised 3D shell models, we manually created another four shell
488 models by transforming three out of the four retopologised NURBS surface 3D shell models by
489 using the “Transform” function in Blender. These models are: 1) *Plectostoma laidlawi* that was
490 resized to half the original size and given slight modification of the aperture size (Figure 2E); 2)
491 *Plectostoma christae* that was reshaped into an elongated form by reducing the model size (linear
492 dimension) to one-half along the x and y axes, and by doubling the size along the z axis (Figure
493 2F); 3) *Plectostoma christae* that was reshaped into a depressed form by multiplying by 1.5 the
494 model size along the x and y axes, and by reducing to one-half along the z axis (Figure 2G); and
495 4) *Opisthostoma vermiculum* that consists of one *Opisthostoma vermiculum* original 3D model of
496 which we connected the aperture to another, enlarged, *Opisthostoma vermiculum* (Figure 2H).
497 Finally, we analysed all these eight shell models by following the procedures 5 to 8.

498 **Results and Discussion**

499 **Retopologised 3D shell models**

500 All the final retopologised 3D shell models can be found in Supplementary Information (Files 7
501 to 14) in PLY ASCII mesh format, with the raw data as a list of vertices, followed by a list of
502 polygons, which can be accessed directly without the need of any 3D software. Each vertex is
503 represented by x, y, z coordinates. Each polygon face consists of four vertices. This simplified yet
504 biologically informative 3D mesh shell model allows the quantification of aperture form and
505 growth trajectory. Moreover, the 3D shell models and their raw vertices data could potentially be
506 used in studies of functional morphology and theoretical modelling of shell form, respectively.

507 Malacologists have been focusing on empirical shell morphological data, from which the
508 functional, ecological and evolutionary aspects were then extracted. The physical properties were
509 then determined by its form (e.g. Okajima & Chiba 2011; Okajima & Chiba, 2012). By using the

510 3D models, the shell properties and function can be analysed *in silico*. For example, the thickness
511 of the shell can be added to the 3D shell model (Figure 3E and Figure 3F) in order to obtain the
512 shell material's volume, the shell's inner volume, its inner and outer surface area, and centre of
513 gravity. We used the "build" function of the software, which can only "solidify" the model by
514 uniform thickness. However, if necessary, it is possible to write a custom Python script to add the
515 desired thickness to the shell. Quantification of shell properties may then be done by using the
516 geometry approach in Meshlab or Blender, as compared to the pre-3D era where mathematical
517 descriptions of the shell form were required (e.g. Moseley, 1838; Raup & Graus, 1972; Stone,
518 1997). Furthermore, it is possible to convert the 3D models to a 3D finite element (FE) model, of
519 which the physical properties (e.g. strength) can be tested (e.g. Faghih Shojaei et al., 2012).

520 In addition to the potential use of 3D shell models in functional morphology, the coordinate data
521 of the vertices of 3D shell models could be used directly by theoretical morphologists (see Figure
522 1 in Urdy et al., 2010). For example, these data can be extracted in different formats that fit the
523 data requirement of different types of theoretical shell models, namely, generating curve models
524 using a fixed reference frame or moving reference frame (Figure 3C), helicospiral or multivector
525 helicospiral models using a fixed reference frame (Figure 3A, Figure 3B and Figure 3D) or
526 growth vector models using a moving reference frame (Figure 3A and Figure 3B).

527 The retopologising of the aperture ontogeny from a raw 3D shell model (procedures 1 to 4) is a
528 time-consuming and tedious process compared with traditional and geometric morphometrics.
529 There are no differences in the time required for data analysis between GM and our method. The
530 only time differences are in the data acquisition. In our experience, two to three days are needed
531 to collect the aperture data from the shell. For example, the four shell models were created by
532 retopologising between 73 and 96 separate apertures (ca. 1500 points for 90 apertures). From the
533 viewpoint of short-term cost-benefit balance, this may be seen as a waste of time, because GM
534 requires not more than a few dozen points for each shell, which can generate the shape variables
535 for a study, even though these points are not comparable to other points of other shells or other
536 studies. However, in the long run, it is a good time investment, since it will allow the
537 understanding of shell function, growth, and evolution, as the same set of data is obtained from
538 different shell forms and can be accumulated and analysed together. Moreover, as with all newly-
539 developed techniques, improvements in efficiency and automation are possible and may remove
540 these impediments in the future.

541 **Comparing shell form from the view of shell ontogeny**

542 Figure 4 gives an overview of the aperture ontogeny profile and shell volume for each species.
543 The curvature, torsion perimeter, and ontogeny axis are represented by true numerical values with
544 the unit of mm^{-1} and mm, and thus can be interpreted directly. In contrast, the aperture shape
545 scores are just statistics of Fourier coefficients and are not the absolute quantification of aperture
546 shape. The PCA score of an aperture shape depends on the shape of other aperture outlines and
547 thus it might change whenever other aperture outlines are added into the analysis. Nevertheless,
548 the aperture scores will stabilise as data of more shells become available and when most of the
549 extreme aperture forms are included. In this study, the first principal component explained 92%
550 of the total variance; the second and third principal component explained only 3% or 1% of the
551 total variance. We showed that the shell form can be represented by the ontogeny changes of the
552 aperture growth trajectory in terms of curvature and torsion, and aperture form, in terms of
553 perimeter and shape.

554 Our first example evaluates this method in illustrating the differences between two shells that
555 have the same shape but differ in shell size – the half-size *Plectostoma laidlawi* (Figure 4E) shell
556 and the original *Plectostoma laidlawi* shell (Figure 4C). As revealed by their aperture ontogeny
557 profiles, the size difference between the two shells has had an effect on the curvature, torsion,
558 ontogeny axis length and aperture size. For the resized *Plectostoma laidlawi* shell, the values of
559 curvature and torsion are twice as large as for the original, whereas the ontogeny axis length and
560 aperture size are only half those of the original shell. However, there is no discrepancy in the
561 aperture shape statistics. Despite this scalar effect, the overall trends in the changes of these
562 variables along the ontogeny axis are comparable between these two shells (Figure 6B).

563 Another example shows the ontogeny profiles of three shells, namely, the elongated (Figure 4G),
564 depressed (Figure 4H), and original (Figure 4A) versions of the *Plectostoma christae* shell.
565 Comparison of aperture profiles among these show the most obvious discrepancies in greater
566 torsion values for the elongated shell, which change in a more dramatic trend along the shell
567 ontogeny. In addition, each of the three shells has its unique aperture shape scores, though there
568 are no big discrepancies in the aperture size. The differences in ontogeny axis length, curvature
569 and torsion are related to the differences of the aperture shape statistics among the three shells.

570 However, our small dataset with only three shells is not sufficient for thorough disentangling of
571 the interplay between aperture size, shape, and growth trajectory in relation to the shell form.

572

573 Our last example is the comparison between the original (Figure 4D) and the composite (Figure
574 4F) *Opisthostoma vermiculum* shell . It is clear that our method has high sensitivity and
575 robustness in the analysis of such bizarre shell forms. As shown in Figure 4F, the start of the
576 aperture ontogeny profile of the composite shell was the same as for the original shell (Figure
577 4D). In addition, the later parts of the ontogeny profile trends are still comparable to the first part,
578 but different in value because of the scalar effect.

579 As an alternative visualisation, Figure 5 shows the radar charts that summarise the same aperture
580 ontogeny profiles of each species. The polygon edges in each chart show how dramatically the
581 aperture form (size and shape), and growth trajectory (curvature and torsion) are changing at each
582 of the subsequent 5% intervals of the shell ontogeny. The aperture size (mm) and the ontogeny
583 segment length (mm) variables indicate the shell size (i.e. volume). To illustrate this, aperture size
584 and ontogeny axis length can be seen as the circle size and height of a cylinder. This chart is
585 useful for the visual comparison between shells that are similar in size, for example, *Plectostoma*
586 *christae* (2.43 mm³), *Plectostoma laidlawi* (2.39 mm³), and the depressed *Plectostoma christae*
587 (2.73 mm³). The radar chart shows that (1) the depressed *Plectostoma christae* is the largest and
588 has a very different aperture shape as compared to the other two shells; (2) most of the shell
589 whorls' form of *Plectostoma christae* is very similar to *Plectostoma laidlawi* (i.e. most of the
590 polygons in the chart were similar), but the *Plectostoma laidlawi* shell differs from *Plectostoma*
591 *christae* shell by having distorted whorls at the last part of the shell ontogeny (magenta lines at
592 torsion) and a more open umbilicus at the beginning of the shell ontogeny (red lines at curvature
593 and aperture size).

594 However, comparison of radar charts between shells that differ greatly in size would be less
595 informative. For example, the radar charts between the resized *Plectostoma laidlawi* shell and the
596 original *Plectostoma laidlawi* shell are very different, though the resized one has the same shell
597 shape as the original. The difference in radar charts between the two shells was therefore mainly
598 caused by the size difference.

599 As we have shown in both graphical techniques (Figures 4 and 5), the shell forms can be
600 explored and compared qualitatively on the basis of aperture ontogeny profiles. Users might need
601 some training in the interpretation of the plots because they are different from both linear
602 dimension measurement plots and geometric morphometric shape coordinate plots. Our
603 evaluation suggested that both data visualisation methods are sensitive and robust in capturing the
604 aperture ontogeny profile for any shell form and thus make the qualitative comparison across
605 gastropod taxa and studies possible.

606 This method could be applied in malacological taxonomy because its core business is the
607 description of shell form. Despite hundreds of years of taxonomic history of shells, there has been
608 little change in the way shell form is being described. For example, shell form is usually
609 described in terms of linear dimensions: shell width and height; number of whorls; shell shape –
610 flat, depressed, globose, conical, or elongated; whorls shape – from flat to convex. Here, we
611 suggest that the aperture ontogeny profiles would be a great supplement to the classical approach
612 to shell description. For example: (1) the size of the shell (its volume) depends on the ontogeny
613 axis length and aperture size; (2) the shell shape depends on the growth trajectory in terms of
614 curvature and torsion; (3) the shape of the whorls depends on the shape of the aperture (Figure 4).
615 In our case of the four shells (Figures 2A – 2D), it is clear that aperture size of each shell is
616 constricted at roughly the same part of the respective shell ontogeny, namely between 70% and
617 85%, regardless of the dissimilar shell sizes and shapes (Figures 4A – 4D, and aperture size
618 profiles in Figure 5B). In fact, these aperture size decreases during ontogeny are in accordance
619 with the shell constriction, one of the shell characters that have been used in the taxonomy of
620 *Opisthostoma* and *Plectostoma* (Vermeulen, 1994; Liew et al., 2014b). However, the shell
621 constriction has not been quantified previously, and we show that it could also be an important
622 developmental homology for the two genera. This preliminary results suggest that these aperture
623 ontogeny profiles could aid the taxonomist in decision-making for grouping taxa based on
624 homologous characters.

625 **Quantitative comparison between different shell forms**

626 Figure 6 shows dendrograms resulting from a permutation distribution clustering analysis of the
627 eight shells in terms of their aperture ontogeny profiles. Figure 6A shows the hierarchical
628 clustering of the eight shells based on all four aperture ontogeny profiles. From this dendrogram,
629 the composite *Opisthostoma vermiculum* is completely separate from the other shells. The

630 remaining seven shells are clustered into two groups. One consists of the more regularly coiled
631 shells, namely, *Plectostoma christae* and its two transformed shells, and *Plectostoma crassipupa*;
632 the other group consists of the shells that deviate from regular coiling, namely *Plectostoma*
633 *laidlawi* and its transformed shell, and *Opisthostoma vermiculum*. Nevertheless, there were high
634 dissimilarities between shells within each group as revealed by the long branch lengths in Figure
635 6A, except for the two *Plectostoma laidlawi* shells (Table 1). The aperture ontogeny profiles for
636 the *Plectostoma laidlawi* shell and its reduced version are almost the same. The high dissimilarity
637 among the other six shells can be explained when each of the variables in the aperture ontogeny
638 profile is analysed separately as shown in Figure 6B.

639 Figure 6B shows the dendrograms of aperture ontogeny profiles for each of the four variables. All
640 four dendrograms have a different topology than the one in Figure 6A. Among the variables, the
641 aperture ontogeny profile of the curvature has the smallest discrepancies among shells. The two
642 *Plectostoma laidlawi* shells are the only pair that clusters together in all the dendrograms of
643 Figures 6A and 6B because they are identical in every aspect of aperture ontogeny profile except
644 torsion. Hence, the independent analysis of aperture ontogeny profile variables corresponds well
645 to the overall analysis of aperture ontogeny profiles.

646 Figure 7 shows a three-dimensional NMDS plot of the distance matrix (Table 1) that was
647 generated from PDC analysis on all four aperture ontogeny profiles. The very low stress level
648 (0.000) indicates that this 3D plot is sufficient to represent the distance matrix of the aperture
649 ontogeny profiles. This NMDS plot can therefore be regarded as a morphospace of the shell
650 shape, as derived from aperture ontogeny profiles. However, neither the dendrogram nor the
651 NMDS plot contains information about the shell size because the analysis of PDC is based on the
652 standardised ontogeny profiles and their trends. Thus, both plots are useful for the comparative
653 analysis of shell shape, but not shell size. Nevertheless, the size comparison between shells is
654 rather straightforward.

655 The conventional quantification of shell size is based on the linear measurement of two or three
656 dimensions of a shell, for example, shell height and shell width. These measurements are
657 extremely effective for size comparisons between similarly-shapes shells. However, the linear
658 measurements have limitations when comparison is made between shells that are different in
659 shape. For example, shell height comparison between a discoidal shell and a fusiform shell tells

660 very little about size differences because the dimensional measurements are tied to a shell shape
661 that results from a different coiling strategy.

662 Thus, shell size may be more appropriately given as shell volume, which can be estimated easily
663 from retopologised 3D shell models (Figure 4). This quantification of shell size in terms of
664 volume is more meaningful from the functional and developmental point of view because a snail
665 should grow a shell in which its entire soft body can fit when the snail withdraws into the shell.
666 In addition to the exact volume, a shorthand to qualitatively comparing size between two shells is
667 by examining the ontogeny axis length and aperture size in the radar chart (Figure 5). We can
668 then compare the form between shells when the dendrograms or NMDS plot are interpreted
669 together with shell size (volume) data. For example, the *Plectostoma laidlawi* shell has the same
670 shape as, but is eight times larger than, the resized *Plectostoma laidlawi*.

671 In addition to the construction of morphospace, the dissimilarity matrix can be used in
672 phylogenetic signal tests (Hardy & Pavoine, 2012). Furthermore, it can also be analysed together
673 with other distance matrices, such as for geographical or ecological distance, to improve our
674 understanding of the evolutionary biology of shell forms.

675 **Conclusions, limitations and future directions**

676 We demonstrated an alternative workflow for data acquisition, exploration and quantitative
677 analysis of shell form. This method has several advantages: (1) robustness – this method can be
678 used to compare any shell form: The same aperture profiles can be obtained from any form of
679 shell. Then, these profiles from different shells and/or different studies can be analysed together.
680 These parameters can be obtained from the aperture as long as the shell grows accretionarily at
681 the aperture; (2) scalability and reproducibility – the data obtained from different studies and
682 different gastropod taxa can be integrated: Aperture ontogeny profiles were obtained from the
683 aperture outlines. This is a trait that exists in every gastropod shell. We believe that the aperture
684 outline that is obtained by multiple experienced malacologists, on different shells, would be
685 highly similar; (3) versatility – outputs from this method are comply with data standard that is
686 required in taxonomy (e.g., functional morphology, theoretical modelling, and evolutionary
687 studies: the raw 3D shell mesh models can be used for visualisation of shells in taxonomic
688 research (e.g. Liew et al., 2014b), coordinates data of the vertices can be used for theoretical

689 modelling (e.g. Urdy et al., 2010), aperture ontogeny profiles can be used for shell functional
690 studies (e.g. Liew & Schilthuizen, 2014), and dissimilarity matrix between shell forms can
691 analysed with phylogenetic distance matrix.

692 Yet, our method has its limitations. Firstly, our retopology procedures rely on a 3D shell model
693 that requires CT-scan technology. In fact, although a CT-scan 3D shell model can certainly
694 facilitate the retopology process of a shell, it is not indispensable. The key of the retopology
695 processes is to digitise the aperture along the shell ontogeny, and thus a shell can be retopologised
696 fully in Blender with a good understanding of the aperture ontogeny profiles by studying the real
697 specimens even without a reference shell model. Secondly, the retopology procedure which is
698 essential for our data acquisition is more time-consuming than traditional and geometric
699 morphometric where data can be obtained from an image taken from a shell. Thirdly, our method
700 is effective in the analysis of overall shell form, but not of the shell ornamentation.

701 In the future, our method can be improved to accommodate the shell ornamentation analysis.
702 Parts of our method (i.e. procedures 1 – 6) can be used to obtain shell ornamentation data, such as
703 radial ribs (*i.e.*, commarginal ribs), but these data cannot be analysed with our qualitative and
704 quantitative approaches that focus on longitudinal growth (i.e. procedures 7 – 8). Finally, we
705 hope this shell form quantification method will simulate more collaboration within malacologists
706 that work in different research fields, and between empirical and theoretical morphologists.

707 **Supplementary Information (<http://dx.doi.org/10.6084/m9.figshare.877061>)**

708 File 1 – Video tutorial for procedure 3 and 4.

709 File 2– A python script for procedures 5 and 6 – Aperture form and growth trajectory analysis on
710 retopologised 3D shell mesh in Blender.

711 File 3– A python script to convert normalised elliptical Fourier coefficients to polygon mesh in
712 Blender.

713 File 4 – Python script for retopologising procedure.

714 File 5 – An R script for data analysis as described in procedures 7 and 8.

715 File 6 – A Blender file consisting of raw data of 8 shells of procedures 1 – 4.

716 File 7 – PLY ASCII mesh 3D model of *Plectostoma laidlawi* Sykes 1902.

717 File 8 – PLY ASCII mesh 3D model of *Plectostoma crassipupa* van Benthem Jutting, 1952.

718 File 9 – PLY ASCII mesh 3D model of *Plectostoma christae* Maassen 2001.
719 File 10 – PLY ASCII mesh 3D model of *Opisthostoma vermiculum* Clements and Vermeulen,
720 2008.
721 File 11 – PLY ASCII mesh 3D model of *Plectostoma laidlawi* that was reduced in size by one-
722 half and with slight modification of the last aperture size.
723 File 12 – PLY ASCII mesh 3D model of *Plectostoma christae* that was reshaped into an elongated
724 form by reducing the model size (linear dimension) by one-half along the x and y axes, and by
725 doubling the size along the z axis.
726 File 13 – PLY ASCII mesh 3D model of *Plectostoma christae* that was reshaped into a depressed
727 form by doubling the model size along the x and y axes, and by reducing the size by one-half
728 along the z axis.
729 File 14 – PLY ASCII mesh 3D model of *Opisthostoma vermiculum* that consists of one
730 *Opisthostoma vermiculum* original 3D model of which the aperture was connected to a second
731 enlarged *Opisthostoma vermiculum*.

732 **Acknowledgments**

733 We are thankful to Heike Kappes, Ton de Winter, Jaap Vermeulen, and Severine Urduy for fruitful
734 discussion. We are grateful to Willem Renema for introducing LTS to CT-Scan instrumentation.
735 Finally, we would like to acknowledge Robert Toonen, Ronald Allan Cruz, and an anonymous
736 reviewer for providing useful comments that improved the manuscript.

737 **Author Contributions**

738 Conceived and designed the experiments: LTS. Performed the experiments: LTS. Analyzed the
739 data: LTS. Contributed reagents/materials/analysis tools: LTS MS. Wrote the paper: LTS MS.

740 **References**

741 Abel RL, Laurini CR, Richter M. 2012. A palaeobiologist's guide to 'virtual' micro-CT
742 preparation. *Palaeontologia Electronica* 15(2):1-16.

743 Ackerly SC. 1989a. Kinematics of accretionary shell growth, with examples from brachiopods
744 and molluscs. *Paleobiology* 15(2):147-164.

- 745 Ackerly SC. 1989b. Shell coiling in gastropods: analysis by stereographic projection. *Palaios*
746 4:374-378
- 747 Andrei RM, Callieri M, Zini MF, Loni T, Maraziti G, Pan MC, Zoppè M. 2012. Intuitive
748 representation of surface properties of biomolecules using BioBlender. *BMC Bioinformatics*,
749 13(Suppl 4):S16.
- 750 Atwood JW, Sumrall CD. 2012. Morphometric investigation of the Pentremites fauna from the
751 Glen Dean formation, Kentucky. *Journal of Paleontology* 86(5):813-828.
- 752 Bayer U. 1978. Morphogenetic programs, instabilities and evolution: a theoretical study. *Neues*
753 *Jahrbuch für Geologie und Paläontologie. Abhandlungen* 156:226-261.
- 754 van Benthem-Jutting WSS. 1952. The Malayan species of *Opisthostoma* (Gastropoda,
755 Prosobranchia, Cyclophoridae), with a catalogue of all the species hitherto described. *The*
756 *Bulletin of the Raffles Museum* 24(5):5-61.
- 757 Van Bocxlaer B, Schultheiß R. 2010. Comparison of morphometric techniques for shapes with
758 few homologous landmarks based on machine-learning approaches to biological discrimination.
759 *Paleobiology* 36(3):497-515.
- 760 Boettiger A, Ermentrout B, Oster G. 2009. The neural origins of shell structure and pattern in
761 aquatic mollusks. *Proceedings of the National Academy of Sciences* 106(16):6837-6842.
- 762 Bookstein FL. 1991. *Morphometric Tools for Landmark Data: Geometry and Biology*.
763 Cambridge University Press.
- 764 Brandmaier AM. 2012a. *Permutation Distribution Clustering and Structural Equation Model*
765 *Trees*. Fakultät 6 - Naturwissenschaftlich-Technische Fakultät I, Universität des Saarlandes.
- 766 Brandmaier AM. 2012b. *pdc: Permutation Distribution Clustering. R package version 0.3*.
767 <http://CRAN.R-project.org/package=pdc>

- 768 Cain AJ. 1977. Variation in the spire index of some coiled gastropod shells, and its evolutionary
769 significance. *Philosophical Transactions of the Royal Society of London. B, Biological Sciences*
770 277:377-428
- 771 Cameron R. 1981. Functional aspects of shell geometry in some British land snails. *Biological*
772 *Journal of the Linnean Society* 16(2):157-167.
- 773 Cardini A, Loy A. 2013. On growth and form in the " computer era": from geometric to biological
774 morphometrics. *Hystrix, the Italian Journal of Mammalogy*, 24(1), 1-5.
- 775 Cassola, VF, de Melo Lima VJ, Kramer R, Khoury HJ. 2010. FASH and MASH: female and male
776 adult human phantoms based on polygon mesh surfaces: I. Development of the anatomy. *Physics*
777 *in Medicine and Biology* 55(1):133.
- 778 Chaplin TA, Yu HH, Rosa MG. 2013. Representation of the visual field in the primary visual area
779 of the marmoset monkey: Magnification factors, point-image size, and proportionality to retinal
780 ganglion cell density. *Journal of Comparative Neurology* 521(5):1001-1019.
- 781 Chacon R. 2012. Using Jacobian elliptic functions to model natural shapes. *International Journal*
782 *of Bifurcation and Chaos* 22(1):1230005.
- 783 Checa A. 1991. Sectorial expansion and shell morphogenesis in molluscs. *Lethaia* 24(1):97-114.
- 784 Checa A, Aguado R. 1992. Sectorial-expansion analysis of irregularly coiled shells: application to
785 the recent gastropod *Distorsio*. *Palaeontology* 35:913-925.
- 786 Cignoni P, Corsini M, Ranzuglia G. 2008. Meshlab: an open-source 3d mesh processing system.
787 *Ercim news* 73:45-46.
- 788 Clarke RK, Grahame J, Mill PJ. 1999. Variation and constraint in the shells of two sibling species
789 of intertidal rough periwinkles (Gastropoda: *Littorina* spp.). *Journal of Zoology* 247(2):145-154.

- 790 Clements R, Liew TS, Vermeulen JJ, Schilthuizen M. 2008. Further twists in gastropod shell
791 evolution. *Biology letters* 4(2):179-182.
- 792 Claude J. 2008. *Morphometrics with R*. Springer.
- 793 Cortie MB. 1989. Models for mollusk shell shape. *South African Journal of Science* 85(7):454-
794 460.
- 795 Cortie MB. 1993. Digital seashells. *Computers & graphics* 17(1):79-84.
- 796 Davoli E, Russo F. 1974. Una metodologia paleontometrica basata sul modello di Raup: Verifica
797 sperimentale su rappresentanti fossili del gen. *Subula* Schumacher. *Bollettino della Societa*
798 *Paleontologica Italiana* 13:108-121.
- 799 Dera G, Eble GJ, Neige P, David B. 2009. The flourishing diversity of models in theoretical
800 morphology: from current practices to future macroevolutionary and bioenvironmental
801 challenges. *Paleobiology* 34 (3):301-317.
- 802 Ekaratne SUK, Crisp DJ. 1983. A geometric analysis of growth in gastropod shells, with
803 particular reference to turbinate forms. *Journal of the Marine Biological Association of the*
804 *United Kingdom* 63(4):777-797.
- 805 Emberton K. 1994. Polygyrid land snail phylogeny: external sperm exchange, early North
806 American biogeography, iterative shell evolution. *Biological Journal of the Linnean Society*
807 52(3): 241-271.
- 808 Evans AR. 2013. Shape descriptors as ecometrics in dental ecology. *Hystrix, the Italian Journal*
809 *of Mammalogy*, 24(1), 8.
- 810 Faghieh Shojaei M, Mohammadi V, Rajabi H, Darvizeh A. 2012. Experimental analysis and
811 numerical modeling of mollusk shells as a three dimensional integrated volume. *Journal of the*
812 *Mechanical Behavior of Biomedical Materials* 16:38-54.

- 813 Foote M, Cowie RH. 1988. Developmental Buffering as a Mechanism for Stasis: Evidence from
814 the Pulmonate *Theba pisana*. *Evolution* 42(2):396-399.
- 815 Fowler DR, Meinhardt H, Prusinkiewicz P. 1992. Modeling seashells. *ACM SIGGRAPH*
816 *Computer Graphics* 26(2):379-387.
- 817 Galbraith C, Prusinkiewicz P, Wyvill B. 2002. Modeling a *Murex cabritii* sea shell with a
818 structured implicit surface modeler. *The Visual Computer* 18(2):70-80.
- 819 Godefroy JE, Bornert F, Gros CI, Constantinesco A. 2012. Elliptical Fourier descriptors for
820 contours in three dimensions: A new tool for morphometrical analysis in biology. *Comptes*
821 *rendus biologiques* 335(3):205-213.
- 822 Goodfriend GA. 1983. Some new methods for morphometric analysis of gastropod shells.
823 *Malacological Review* 16:79-86.
- 824 Graus RR. 1974. Latitudinal trends in the shell characteristics of marine gastropods. *Lethaia*,
825 7(4):303-314.
- 826 Hardy OJ, Pavoine S. 2012. Assessing phylogenetic signal with measurement error: a comparison
827 of Mantel tests, Blomberg et al.'s K, and phylogenetic distograms. *Evolution* 66:2614-2621
- 828 Haug JT, Maas A, Waloszek D. 2009. Ontogeny of two Cambrian stem crustaceans, †*Goticaris*
829 *longispinosa* and †*Cambropachycope clarksoni*. *Palaeontographica A* 289:1-43.
- 830 Haug JT, Waloszek D, Haug C, Maas A. 2010. High-level phylogenetic analysis using
831 developmental sequences: The Cambrian †*Martinssonina elongata*, †*Musacaris gerdgeyeri* gen. et
832 sp. nov. and their position in early crustacean evolution. *Arthropod Structure & Development*
833 39(2):154-173.

- 834 Haug C, Haug JT, Fayers SR, Trewin NH, Castellani C, Waloszek D, Maas A. 2012.
835 Exceptionally preserved nauplius larvae from the Devonian Windyfield chert, Rhynie,
836 Aberdeenshire, Scotland. *Palaeontologia Electronica* 15:2-24.
- 837 Harary G, Tal A. 2011. The natural 3D spiral. *Computer Graphics Forum* 30(2):237-246.
- 838 Hutchinson J. 1999. But which morphospace to choose?: Theoretical Morphology by GR
839 McGhee, Jr. *Trends in Ecology & Evolution* 14:414.
- 840 Iller C. 1983. The mathematics of gnomonic seashells. *Mathematical Biosciences* 63:21-56.
- 841 Illert C, Pickover CA. 1992. Generating irregularly oscillating fossil seashells. *Computer*
842 *Graphics and Applications, IEEE* 12(3):18-22.
- 843 Im CH, Park JH, Shim M, Chang WH, Kim YH. 2012. Evaluation of local electric fields
844 generated by transcranial direct current stimulation with an extracephalic reference electrode
845 based on realistic 3D body modeling. *Physics in Medicine and Biology* 57(8):2137.
- 846 Johnston MR, Tabachnick RE, Bookstein FL. 1991. Landmark-based morphometrics of spiral
847 accretionary growth. *Paleobiology* 17(1):19-36.
- 848 Kaesler RL, Waters JA. 1972. Fourier analysis of the ostracode margin. *Geological Society of*
849 *America Bulletin* 83(4):1169-1178.
- 850 Kawaguchi Y. 1982. A morphological study of the form of nature. *Computer Graphics* 16:223-
851 232.
- 852 Klingenberg CP. 2013. Visualizations in geometric morphometrics: how to read and how to make
853 graphs showing shape changes. *Hystrix, the Italian Journal of Mammalogy*, 24(1), 10.
- 854 Kohn AJ, Riggs AC. 1975. Morphometry of the *Conus* shell. *Systematic Zoology* 24:346-359.

- 855 Kuhl FP, Giardina CR. 1982. Elliptic Fourier features of a closed contour. *Computer Graphics*
856 *and Image Processing* 18(3):236-258.
- 857 Lewiner T, Gomes Jr JD, Lopes H, Craizer M. 2005. Curvature and torsion estimators based on
858 parametric curve fitting. *Computers & Graphics* 29(5):641-655.
- 859 Liew TS, Kok ACM, Urdy S, Schilthuizen M. 2014a. On growth and form of irregular coiled-
860 shell of a terrestrial snail: *Plectostoma concinnum* (Fulton, 1901) (Mollusca: Caenogastropoda:
861 Diplommatinidae). *PeerJ* 2:e383.
- 862 Liew TS, Schilthuizen M. 2014. Association between shell morphology of micro-land snails
863 (genus *Plectostoma*) and their predator's predatory behaviour. *PeerJ* 2:e329
- 864 Liew T-S, Vermeulen JJ, Marzuki ME, Schilthuizen M. 2014b. A cybertaxonomic revision of the
865 terrestrial micro-landsnail genus *Plectostoma* Adam (Mollusca, Caenogastropoda,
866 Diplommatinidae), from Peninsular Malaysia, Sumatra and Indochina. *Zookeys* 393:1-107.
- 867 Løvtrup S, von Sydow B. 1974. D'Arcy Thompson's theorems and the shape of the molluscan
868 shell. *Bulletin of Mathematical Biology* 36:567-575.
- 869 Lv Z, Tek A, Da Silva F, Empereur-mot C, Chavent M, Baaden M. 2013. Game On, Science-How
870 Video Game Technology May Help Biologists Tackle Visualization Challenges. *PLoS ONE*
871 8(3):e57990.
- 872 Maassen WJM. 2001. Four new Diplommatinidae (Gastropoda, Prosobranchia,
873 Diplommatinidae) from southern Thailand and northern Peninsular Malaysia. *Basteria* 65(1-
874 3):51-56.
- 875 Mayer G, Haug J, Maas A, Waloszek D. 2012. Functional aspects of the gammaridean mandibles
876 with special reference to the *lacinia mobilis* (Crustacea, Amphipoda). *Zoologischer Anzeiger-A*
877 *Journal of Comparative Zoology* 252:536-547.

- 878 McGhee GR. 1978. Analysis of the shell torsion phenomenon in the Bivalvia. *Lethaia* 11(4):315-
879 329.
- 880 McGhee GR. 1999. *Theoretical Morphology: the Concept and Its Applications*. Columbia
881 University Press.
- 882 McGhee GR. 2007. *The Geometry of Evolution: Adaptive Landscapes and Theoretical*
883 *Morphospaces*. New York: Cambridge University Press.
- 884 Meinhardt H. 2009. *The Algorithmic Beauty of Sea Shells*. Springer.
- 885 Monnet C, Zollikofer C, Bucher H, Goudemand N. 2009. Three-dimensional morphometric
886 ontogeny of mollusc shells by micro-computed tomography and geometric analysis.
887 *Paleontologia Electronica* 12(3/12A):1-13.
- 888 Moseley H. 1838. On the geometrical forms of turbinated and discoid shells. *Philosophical*
889 *Transactions of the Royal Society of London* 128:351-370.
- 890 Moulton DE, Goriely A. 2012. Surface growth kinematics via local curve evolution. *Journal of*
891 *mathematical biology*: 1-28.
- 892 Moulton DE, Goriely A, Chirat R. 2012. Mechanical growth and morphogenesis of seashells.
893 *Journal of Theoretical Biology* 311:69-79.
- 894 Nakazawa M. 2012. *fmsb: Functions for Medical Statistics Book with Some Demographic Data*.
895 *R package version 0.4.1*. <http://CRAN.R-project.org/package=fmsb>
- 896 Newkirk GF, Doyle RW. 1975. Genetic analysis of shell-shape variation in *Littorina saxatilis* on
897 an environmental cline. *Marine Biology* 30(3):227-237.
- 898 Noshita K. 2010. Spiral Shell Form: A computer software package for theoretical morphological
899 analysis of spiral shell form. *Geoscience reports of Shizuoka University* 37:57-73. (In Japanese)

- 900 Okajima R, Chiba S. 2011. How does life adapt to a gravitational environment? The outline of the
901 terrestrial gastropod shell. *The American Naturalist* 178(6):801-809.
- 902 Okajima R, Chiba S. 2012. Adaptation from restricted geometries: the shell inclination of
903 terrestrial gastropods. *Evolution* 67:429-437.
- 904 Okamoto T. 1988. Analysis of heteromorph ammonoids by differential geometry. *Palaeontology*
905 31(1):35-52.
- 906 Oliphant TE. 2007. Python for scientific computing. *Computing in Science & Engineering*
907 9(3):10-20.
- 908 Picado J. 2009. Seashells: the plainness and beauty of their mathematical description. *MAA*
909 *Mathematical Sciences Digital Library*: 1-18.
- 910 Pyka M, Hertog M, Fernandez R, Hauke S, Heider D, Dannlowski U, Konrad C. 2010. fMRI data
911 visualization with BrainBlend and Blender. *Neuroinformatics* 8(1):21-31.
- 912 R Core Team. 2013. *R: A Language and Environment for Statistical Computing*. R Foundation
913 for Statistical Computing, Vienna, Austria. URL <http://www.R-project.org/>.
- 914 RStudio. 2012. *RStudio: Integrated Development Environment for R* (Version 0.97.336), Boston,
915 MA. URL <http://www.rstudio.org/>.
- 916 Raup DM. 1961. The geometry of coiling in gastropods. *Proceedings of the National Academy of*
917 *Sciences of the United States of America* 47(4):602.
- 918 Raup DM. 1967. Geometric analysis of shell coiling: coiling in ammonoids. *Journal of*
919 *Paleontology* 41(1):43-65.
- 920 Raup DM, Graus RR. 1972. General equations for volume and surface area of a logarithmically
921 coiled shell. *Journal of the International Association for Mathematical Geology* 4:307-316.

- 922 Raup DM, Michelson A. 1965. Theoretical morphology of the coiled shell. *Science*
923 147(3663):1294-1295.
- 924 Rice SH. 1998. The bio-geometry of mollusc shells. *Paleobiology* 24(1):133-149.
- 925 Rohlf FJ, Archie JW. 1984. A comparison of Fourier methods for the description of wing shape in
926 mosquitoes (Diptera: Culicidae). *Systematic Biology* 33(3):302-317.
- 927 Rohlf FJ, Slice D. 1990. Extensions of the Procrustes method for the optimal superimposition of
928 landmarks. *Systematic Biology* 39(1):40-59.
- 929 Samadi S, David P, Jarne P. 2000. Variation of shell shape in the clonal snail *Melanoides*
930 *tuberculata* and its consequences for the interpretation of fossil series. *Evolution* 54(2):492-502.
- 931 Sarkar D. 2008. *Lattice: Multivariate Data Visualization with R*. Springer.
- 932 Saunders WB, Shapiro EA. 1986. Calculation and simulation of ammonoid hydrostatics.
933 *Paleobiology* 12(1):64-79.
- 934 Savazzi E. 1985. SHELLGEN: A BASIC program for the modeling of molluscan shell ontogeny
935 and morphogenesis. *Computers & Geosciences* 11(5):521-530.
- 936 Savazzi E. 1990. Biological aspects of theoretical shell morphology. *Lethaia* 23(2):195-212.
- 937 Savazzi E. 1992. Shell construction, life habits and evolution in the gastropod *Velates*.
938 *Palaeogeography, Palaeoclimatology, Palaeoecology* 99(3):349-360.
- 939 Savazzi E. 1993. C++ classes for theoretical shell morphology. *Computers & Geosciences* 19(7):
940 931-964.
- 941 Savazzi E. 1995. Theoretical shell morphology as a tool in construction morphology. *Neues*
942 *Jahrbuch für Geologie und Paläontologie. Abhandlungen* 195:229-240.

- 943 Schindel DE. 1990. Unoccupied morphospace and the coiled geometry of gastropods:
944 architectural constraint or geometric covariation. In Ross, R. M. and Allmon W. D. (eds) *Causes*
945 *of Evolution: A Paleontological Perspective*. University of Chicago Press, Chicago. Page 270-
946 304.
- 947 Sykes ER. 1902. Descriptions of six new land shells from the Malay Peninsula. *Journal of*
948 *Malacology* 9:22-23.
- 949 Stepień C. 2009. An IFS-based method for modelling horns, seashells and other natural forms.
950 *Computers & Graphics* 33(4):576-581.
- 951 Stone JR. 1997. Mathematical determination of coiled shell volumes and surface areas. *Lethaia*
952 30:213-219.
- 953 Tissot BN. 1988. Geographic variation and heterochrony in two species of cowries (genus
954 *Cypraea*). *Evolution* 42(1):103-117.
- 955 Ubukata T. 2001. Stacking increments: a new model and morphospace for the analysis of bivalve
956 shell growth. *Historical Biology: A Journal of Paleobiology* 15(4):303-321.
- 957 Urdy S, Goudemand N, Bucher H, Chirat R. 2010. Allometries and the morphogenesis of the
958 molluscan shell: a quantitative and theoretical model. *Journal of Experimental Zoology Part B:*
959 *Molecular and Developmental Evolution* 314(4):280-302.
- 960 Venables WN, Ripley BD. 2002. *Modern Applied Statistics with S*. Springer.
- 961 Verduin A. 1982. How complete are diagnoses of coiled shells of regular build? A mathematical
962 approach. *Basteria* 45(6):127-142.
- 963 Vermeij GJ. 1971. Gastropod evolution and morphological diversity in relation to shell geometry.
964 *Journal of Zoology* 163(1):15-23.

- 965 Vermeulen JJ. 1994. Notes on the non-marine molluscs of the island of Borneo. 6. The genus
966 *Opisthostoma* (Gastropoda Prosobranchia: Diplommatinidae), part 2. *Basteria* 58(3-4): 73-191.
- 967 Warburton K. 1979. Variation in shell geometry in the genus *Lacuna* (Prosobranchia: Lacunidae).
968 *Journal of Natural History* 13(3):385-391.

Table 1 (on next page)

Table 1. Dissimilarity matrix of aperture ontogeny profiles of eight shells obtained from Permutation Distribution Clustering.

Table 1. Dissimilarity matrix of aperture ontogeny profiles of eight shells obtained from Permutation Distribution Clustering.

Shell	(1)	(2)	(3)	(4)	(5)	(6)	(7)	(8)
(1) <i>Plectostoma laidlawi</i>	0.00							
(2) <i>Plectostoma crassipupa</i>	2.44	0.00						
(3) <i>Plectostoma christae</i>	2.65	2.83	0.00					
(4) <i>Opisthostoma vermiculum</i>	2.63	2.56	2.59	0.00				
(5) half-sized <i>P. laidlawi</i>	2.69	2.80	0.09	2.55	0.00			
(6) composite <i>O. vermiculum</i>	3.12	3.48	3.40	3.39	3.34	0.00		
(7) elongated <i>P. christae</i>	2.09	2.55	3.03	2.79	3.03	3.36	0.00	
(8) depressed <i>P. christae</i>	2.01	2.73	3.16	2.94	3.21	3.84	2.62	0.00

Figure 1

Procedures to generate a retopologised shell based on the aperture ontogeny from a shell by using Blender software.

(A) Procedure 3 - Creating reference: Tracing aperture from shell model. (B) Procedure 3 - Creating reference: Tracing ontogeny axis. (C) Procedure 3 – both traced aperture outline and ontogeny axis were converted to Bezier curves. (D) Procedure 4 – Retopologising aperture outlines from the reference by using NURBS circles in EDIT mode. (E) Retopologised aperture outlines. (F) Procedure 4 – Generating retopologised shell surface models from NURBS circles in EDIT mode. (G) Final retopologised NURBS surface shell model. (H) Retopologised 3D shell mesh converted from retopologised NURBS surface shell model.

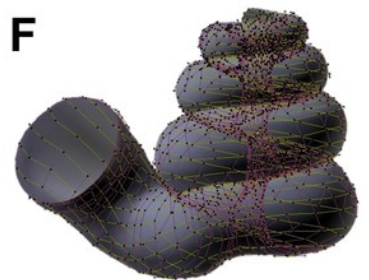
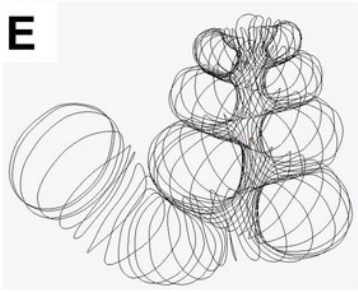
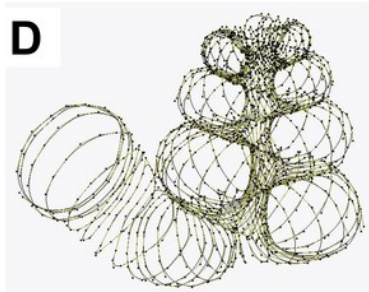
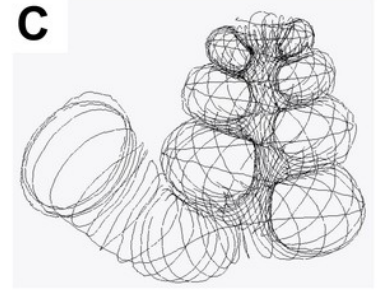


Figure 2

Retopologised shell 3D models obtained by reopotologising real shells (A – D) and by transformation of retopologised shells (E – H).

(A) Shell of *Plectostoma laidlawi* (Sykes 1902). (B) Shell of *Plectostoma crassipupa* (van Benthem Jutting), 1952. (C) Shell of *Plectostoma christae* (Maassen 2001). (D) Shell of *Opisthostoma vermiculum* Clements and Vermeulen, 2008. (E) *Plectostoma laidlawi* shell that was resized by one-half and with slight modification of the last aperture size. (F) *Plectostoma christae* shell that was reshaped into an elongated form by reducing the model size (linear dimension) by one-half along the x and y axes, and by doubling the size along the z axis. (G) *Plectostoma christae* shell that was reshaped into a depressed form by increasing by 1.5 the model size along the x and y axes, and by reducing the size by one-half along the z axis. (H) *Opisthostoma vermiculum* shell that consists of one *Opisthostoma vermiculum* original 3D model of which the aperture was connected to a second, enlarged, *Opisthostoma vermiculum*.

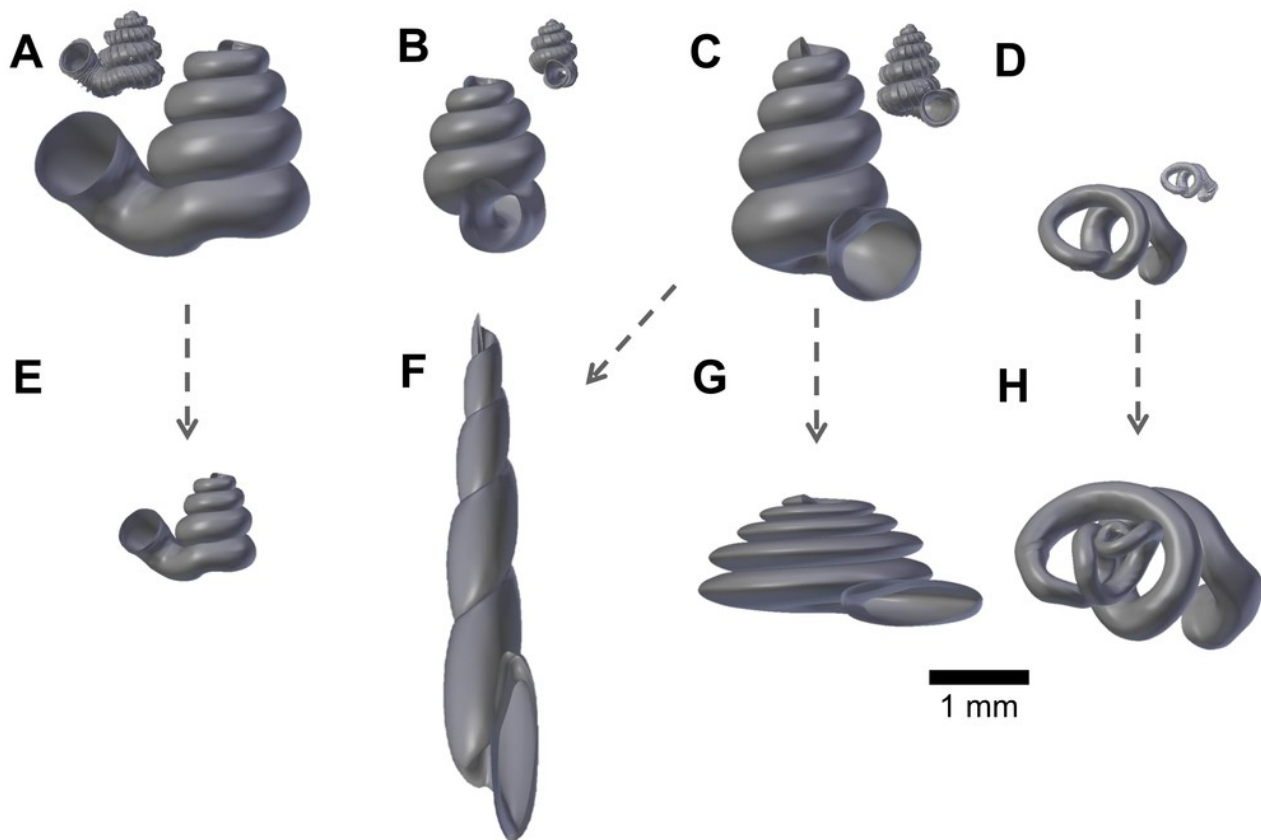


Figure 3

Different data types that could be obtained directly from a 3D shell model that was retopologised on the basis of the aperture ontogeny.

(A) Aperture maps (*sensu* Rice, 1998) or growth vector maps (*sensu* Urdy et al., 2010). (B) same as (A), but the data can be obtained in a greater resolution. (C) Aperture outlines data for generating curve models. (D) Multiple ontogeny axes for helicospiral models. (E) Simple 3D surface shell model with no thickness. (F) 3D surface shell model with added thickness.

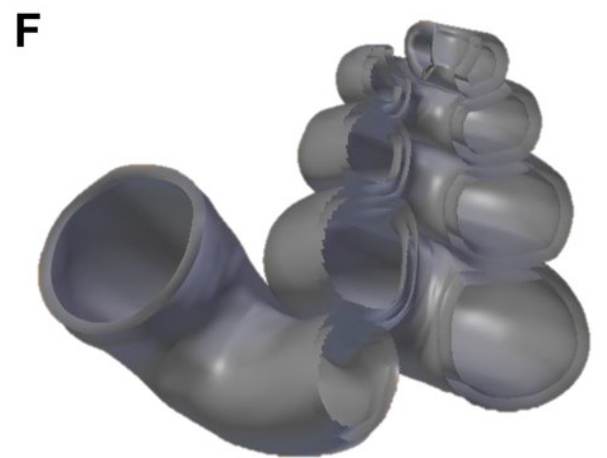
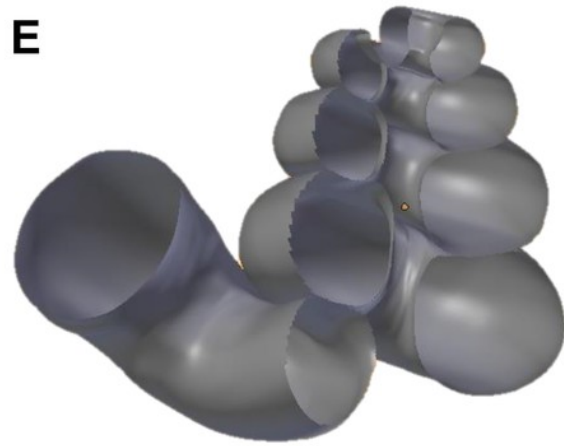
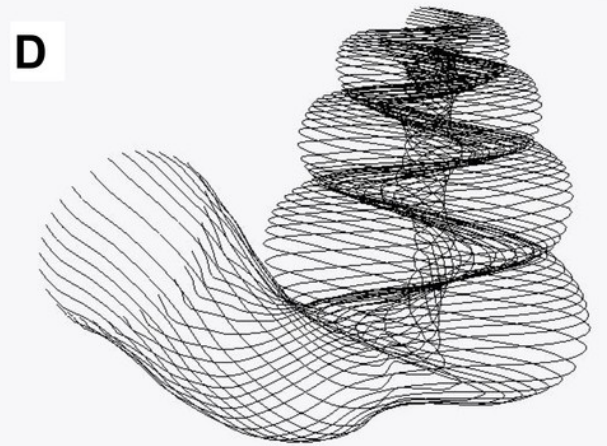
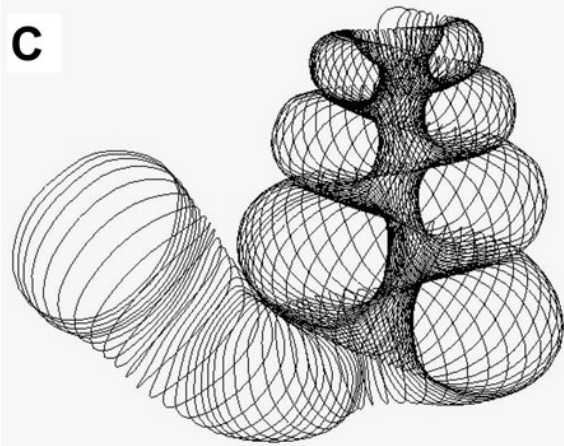
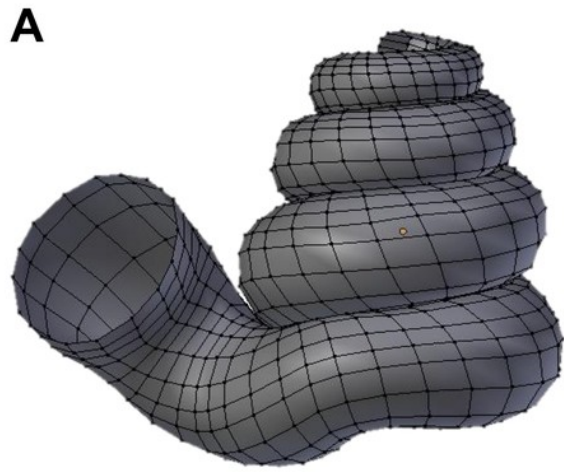


Figure 4

Shell size (volume) and aperture ontogeny profiles in terms of aperture growth trajectory (curvature and torsion) and aperture form (size and shape) of eight shells.

(A) Shell of *Plectostoma christae* (Maassen 2001). (B) Shell of *Plectostoma crassipupa* (van Benthem Jutting, 1952). (C) Shell of *Plectostoma laidlawi* (Sykes 1902). (D) Shell of *Opisthostoma vermiculum* Clements and Vermeulen, 2008. (E) *Plectostoma laidlawi* shell that was resized by one-half and with slight modification of the last aperture size. (F) *Opisthostoma vermiculum* shell that consists of one *Opisthostoma vermiculum* original 3D model of which the aperture was connected to a second enlarged *Opisthostoma vermiculum*. (G) *Plectostoma christae* shell that was reshaped into an elongated form by reducing the model size (linear dimension) by one-half along the x and y axes, and by doubling the size along the z axis. (H) *Plectostoma christae* shell that was reshaped into a depressed form by increasing by 1.5 of the model size along the x and y axes, and by reducing the size by one-half along the z axis.

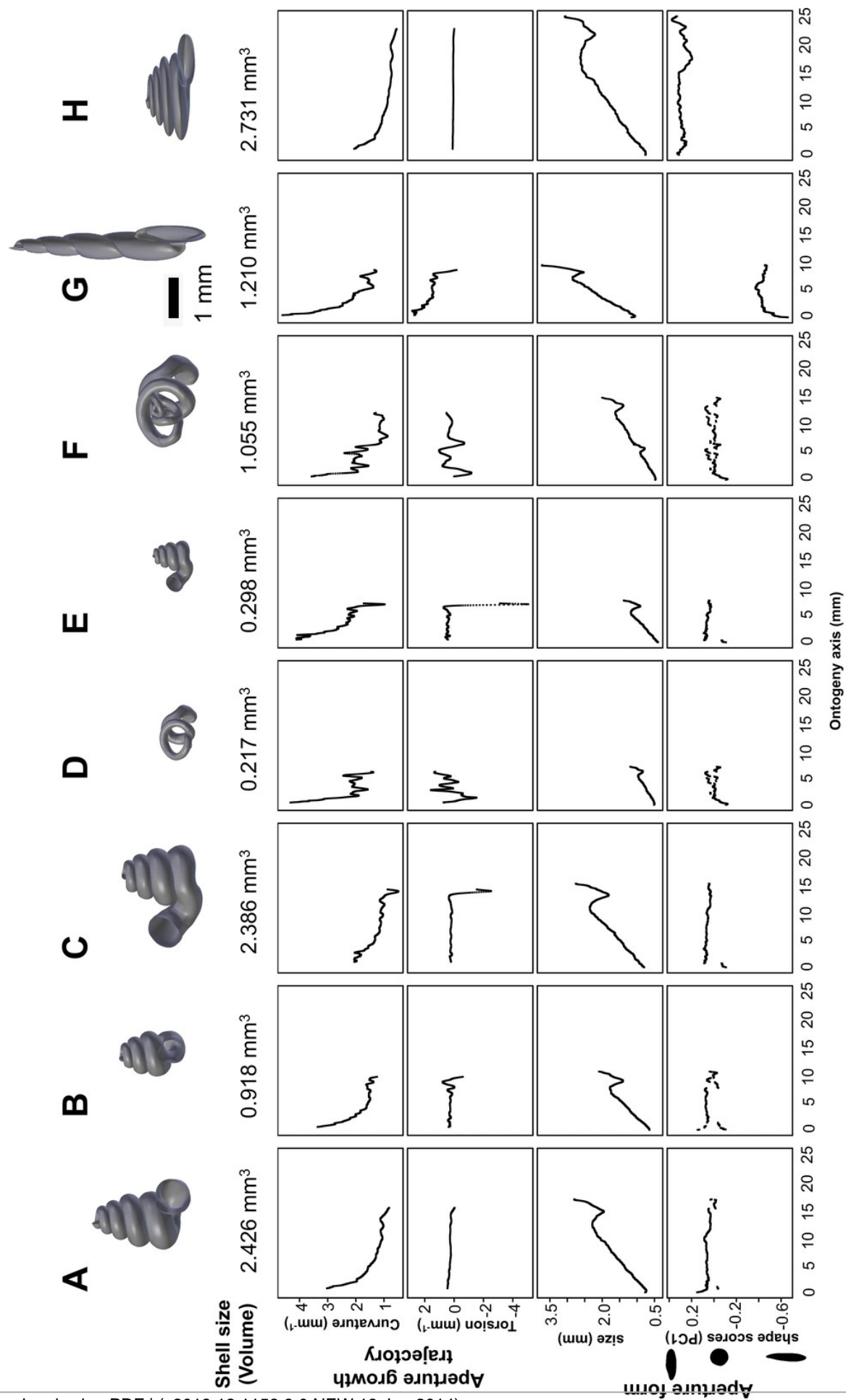


Figure 5

Radar charts of the aperture ontogeny profiles of eight shells.

Each radar chart shows the value and trends of the curvature, torsion, aperture size, aperture shape scores, and ontogeny axis length of each shell.

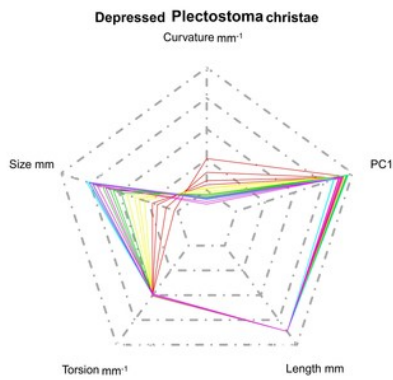
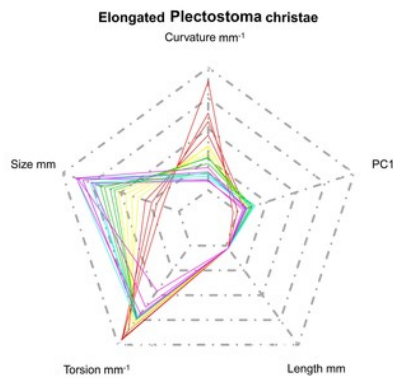
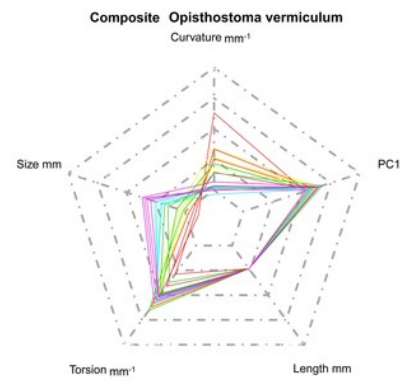
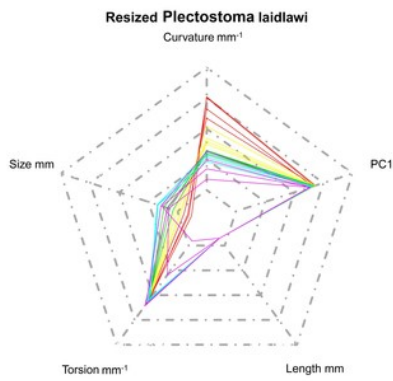
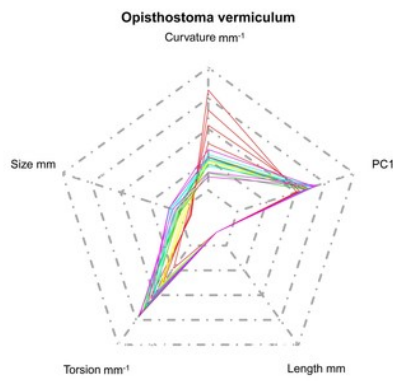
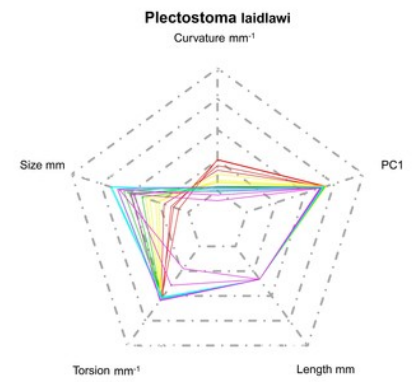
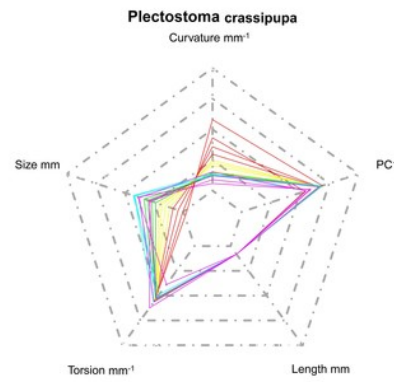
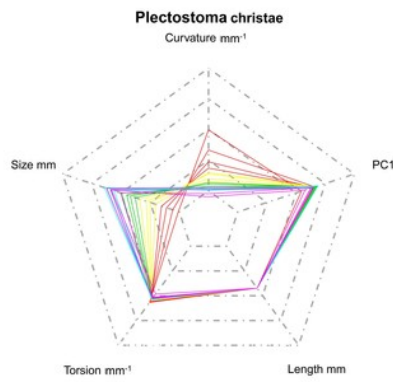
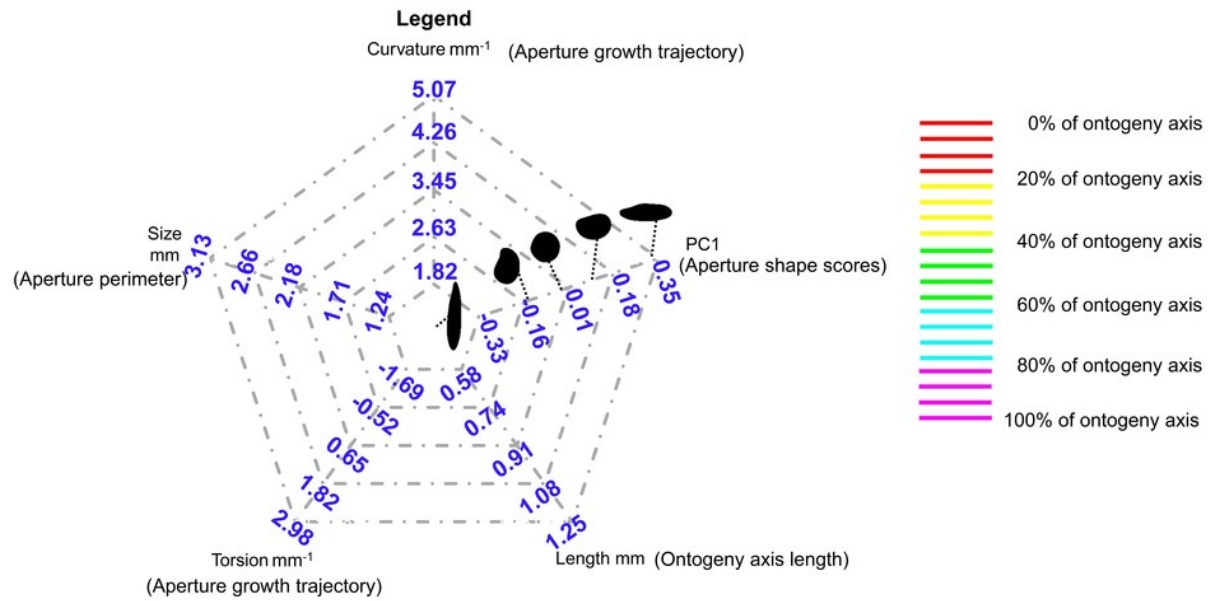


Figure 6

Dendrogram from permutation distribution clustering of the aperture ontogeny profiles of eight shells.

(A) Dendrogram from permutation distribution clustering of the four aperture ontogeny profiles, namely, curvature, torsion, aperture size, and aperture shape scores, of eight shells.

(B) Four dendrograms from permutation distribution clustering of eight shells, which each for the four aperture ontogeny profiles, namely, curvature, torsion, aperture size, and aperture shape scores.

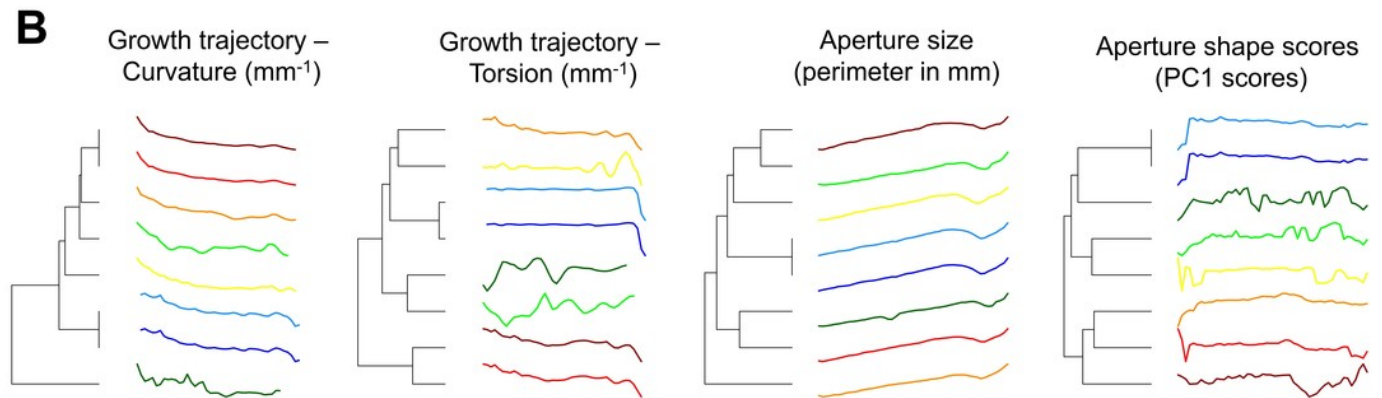
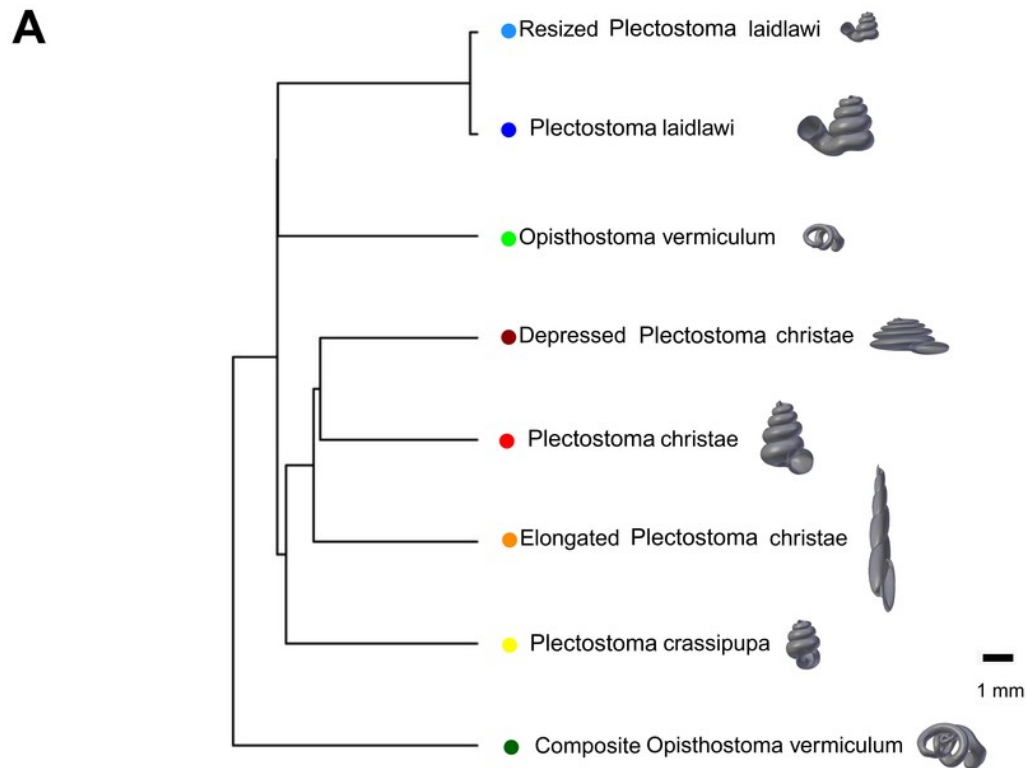


Figure 7

Non-metric multidimensional scaling (NMDS) 3D plots as shell morphospace.

The NMDS plots were generated from a dissimilarity matrix of eight *Opisthostoma* shells aperture ontogeny profiles, which were analysed by permutation distribution clustering.

